APOE4 expression confers a mild, persistent reduction in neurovascular function in the visual cortex and hippocampus of awake mice

*Orla Bonnar[+], Kira Shaw[+], Dori M. Grijseels, Devin Clarke, Laura Bell, Silvia Anderle, Sarah L. King & Catherine N. Hall**

All affiliations: School of Psychology and Sussex Neuroscience, University of Sussex, Falmer, Brighton, East Sussex, BN1 9RH

[+] These authors contributed equally to this work

*****For correspondence, please contact Catherine.hall@sussex.ac.uk

Abstract

Young mice possessing the e4 allele of the Apolipoprotein (APOE) gene (a risk factor for Alzheimer's disease (AD)) have previously been shown to have dramatic decreases in vascular function, suggesting APOE4 may confer its risk via the vasculature. However, in human carriers, vascular and cognitive function decrease later in life. Mouse data may be confounded by an increased impact of anaesthesia and surgery in APOE4 animals, and has also focused on sensory cortices, ignoring medial lobe structures more sensitive to AD.

To clarify how APOE4 expression alters neurovascular function, we studied the visual cortex and hippocampus of awake APOE3 and APOE4 targeted replacement mice, using 2-photon microscopy of neurons and blood vessels.

We found milder vascular deficits than studies using anaesthetised preparations: functional hyperaemia was unaffected in APOE4 mice and neuronal or vascular function did not decrease with age. Instead, vascular responsiveness was lower at all ages, arteriole vasomotion was reduced and neuronal calcium signals during visual stimulation were increased. This suggests that, independently, APOE4 expression is not catastrophic but alters neurovascular physiology towards a state more sensitive to insults such as surgery or beta amyloid accumulation. Understanding how APOE4 expression interacts with these insults will be critical for understanding the emergence of AD in APOE4 carriers.

Introduction

The brain's dense network of vasculature performs a myriad of roles that are crucial for neuronal health and function, including the fine-tuned delivery of oxygen and glucose via the blood, in response to neuronal activity (neurovascular coupling), and the clearance of waste products from the brain, including beta amyloid (Aβ). Both these processes require controlled constriction and dilation of microvascular smooth muscle cells and pericytes. In neurovascular coupling, this likely matches blood flow to energy demand (Iadecola, 2017), while perivascular clearance along blood vessels is promoted by slow (~0.1Hz) oscillations of arterioles, termed vasomotion (Aldea et al., 2019; van Veluw et al., 2020). Alterations to these processes are associated with several neurodegenerative diseases, including Alzheimer's disease (AD). In AD, these changes in cerebral blood flow likely establish a vicious cycle that exacerbates AD pathology, whereby decreased blood flow increases Aβ accumulation by promoting its formation in hypoxic conditions. Blood flow is then limited by accumulating Aβ, as blood vessels are constricted by soluble Aβ, and accumulation of Aβ within vessels likely inhibits vasomotion (Di Marco et al., 2015; Hamilton et al., 2010; Kisler et al., 2017; Sun et al., 2006; van Veluw et al., 2020). Vascular dysregulation has been shown to be among the earliest pathologies found in AD (Iturria-Medina et al., 2016), so disrupted blood flow may be the primary cause of emerging AD pathology.

Recent work from our group has demonstrated heterogeneity in vascular function across brain regions, where CA1 region of the hippocampus was less able to match blood supply to neuronal demand compared to the primary visual cortex (Shaw et al., 2021a). Such regional variability follows not only the known differences in vulnerability to hypoxia (Michaelis, 2012), but is also congruent with regional susceptibility in AD, where sensory cortices are relatively spared compared to the hippocampus. It is therefore possible that the weaker neurovascular function in the hippocampus could contribute to its earlier damage during AD.

Whilst the majority of AD cases are sporadic, the risk of going on to develop the disease is increased 9-15 fold by the possession of an ε4 allele of the apolipoprotein E (APOE) gene (Corder et al., 1993; Yamazaki et al., 2019). ApoE is a protein involved in the transport of lipids and is produced primarily by astrocytes in the central nervous system, but also by vascular mural cells and microglia, as well as by neurons under stress conditions, (Yamazaki et al., 2019). APOE4 expression exacerbates multiple features of AD, increasing Aβ accumulation and tau phosphorylation and altering synaptic function (Najm et al., 2019)(Yamazaki et al., 2019). It also decreases blood brain barrier (BBB) integrity and causes pericyte damage in animal models and human subjects (Bell et al., 2012); (Montagne et al., 2020);). Additionally, in anaesthetised mice, APOE4 mice had reduced cerebral blood flow (CBF) and smaller increases in CBF after sensory stimulation (Bell et al., 2012); (Koizumi et al., 2018).

Because in humans, CBF changes occur before any other AD pathology (Iturria-Medina et al., 2016), such APOE4-mediated vascular dysfunction could be an important contributor to the earlier emergence of AD in APOE carriers. However, gaps in the data remain, complicating understanding of how APOE4 genotype could be promoting AD.

Firstly, neuronal activity has largely not been studied concurrently with vascular function and reports as to the impact of APOE4 genotype on neuronal activity are variable. Large decreases in neuronal activity have been reported in mice aged only 4 months (Bell et al., 2012), but neuronal hyperactivity

has been reported in old APOE4 mice (Nuriel et al., 2017). The potential direction of causality is therefore unclear: could decreases in CBF be due to decreased neuronal drive or could they themselves be restricting neuronal function?

Secondly, the impact of APOE4 on neurovascular coupling in the hippocampus has not yet been studied, despite it being more sensitive to AD damage (Henneman et al., 2009), a site of BBB breakdown in old APOE4 carriers (Montagne et al., 2020) and having weaker neurovascular function than more studied neocortical regions (Shaw et al., 2021a).

Finally, animal studies in which CBF and functional hyperaemia are dramatically decreased in young mice (Bell et al., 2012; Koizumi et al., 2018)do not recapitulate the human condition in which young APOE4 carriers show, if anything, increased CBF compared to APOE3 carriers from young into early old age (Thambisetty et al., 2010; Wierenga et al., 2013). BBB changes in human APOE4 carriers have also only been reported from old age (Halliday et al., 2016; Montagne et al., 2020), whereas these changes were observed in very young mice (Bell et al., 2012). It is therefore hard to interpret the relevance of rodent studies that show much more extreme changes in young animals (Bell et al., 2012; Koizumi et al., 2018) than are seen in humans.

An explanation for the greater impact of APOE4 in rodent studies than humans may be that carrying APOE4 increases the impact of stressors such as anaesthesia (Browndyke et al., 2021; Schenning et al., 2016). Inhalation anaesthetics such as isoflurane - the anaesthetic used in several of the rodent studies – seem to have a particularly large effect, reducing cognitive function acutely after surgery, before recovering to baseline levels after 10 days (Cai et al., 2012).

To plug these gaps in our understanding of how APOE4 impacts on cerebrovascular function, we therefore studied awake mice expressing human APOE3 or 4 in place of murine APOE, to avoid the confounding effect of acute surgery and anaesthesia. We did this by implanting mice with a chronic cranial window and recording neurovascular function up to 4 months after mice recovered from surgery, tracking function from young age to late middle age. To unpick the contribution of neurons and blood vessels to any alterations in neurovascular function we used 2-photon imaging to measure neuronal and vascular activity at a single vessel and neuronal level, as well as measuring the summed activity of neuronal metabolism and vasodilation using haemoglobin spectrometry and laser doppler flowmetry. Finally, we studied both the primary visual cortex (V1) and the CA1 subfield of the hippocampus to probe whether APOE4 effects were more pronounced in the hippocampus given its sensitivity to AD and weaker basal neurovascular function.

Instead of the dramatic reductions in CBF that were reported in acutely anaesthetised experiments, we observed several subtle yet persistent alterations in neurovascular function that persisted from young to late middle age, including impaired vasomotion, neuronal hyperactivity and less reliable vascular responses to neuronal activation. These data are more consistent with the pattern of results observed in humans than in anaesthetised mice, and suggest APOE4 genotype does not itself catastrophically impair vascular function but rather more subtly shifts neurovascular physiology such that it is more susceptible to further insults (e.g. surgery, ageing or beta amyloid accumulation).

121 **Results**

122 **Reduced vascular density in young APOE4-TR mice is not reflected in baseline flow and blood**
123 **oxygenation.**

124 Studies using anaesthetised preparations have previously shown decreased vascular density and
125 cerebral blood flow in APOE4 compared to APOE3 TR mice (Bell et al., 2012); (Koizumi et al., 2018). We
126 confirmed the reduction in vascular density in the visual cortex and HC of 3-4 month APOE4-TR mice
127 using fixed brain tissue with the vasculature filled with a fluorescent gelatin (Fig. 1A, B). As previously
128 (Shaw et al., 2021a), we also observed a reduced vascular density in HC compared to V1. The combined
129 effect of the regional and genotype effects was that the vascular density in APOE4 mice HC was less
130 than half that in APOE3 V1, suggesting potentially compromised function in APOE4 HC.

131 We then investigated the impact this reduction in vascular density had on various aspects of
132 haemodynamic function, using awake head-fixed mice with either a cranial window implanted over the
133 visual cortex or a cannula implanted over CA1 (Shaw et al., 2021a), at rest and in the absence of visual
134 stimulation (hereafter referred to as 'baseline' conditions; Fig. 1C). Surprisingly, there were minimal
135 differences in resting haemodynamics between genotypes, despite the large difference in vascular
136 densities. Studying individual vessels using 2 photon microscopy, baseline red blood cell velocity
137 (RBCV; Fig. 1D, E) and haematocrit (Fig. 1D, G) did not differ between genotypes or brain region, nor
138 did the diameters of individual capillaries (Fig. 1H). The coefficient of variation (CV; calculated by
139 dividing the standard deviation over time by the mean), reflecting temporal fluctuations in RBCV, was
140 lower in HC than in V1 (Fig. 1F), suggesting more homogenous flow. This may promote oxygen
141 extraction (Angleys et al., 2015) in hippocampal vessels, compensating for the lower hippocampal CBF.
142 Conversely, flow was more variable in APOE4 than APOE3 vessels in both brain regions which may
143 indicate less efficient oxygen extraction in APOE4 mice.

144 Macroscopic flow properties assessed using combined haemoglobin spectroscopy and laser doppler
145 flowmetry also, however, revealed no differences between genotypes in RBC flux, total haemoglobin
146 (HbT), oxygen saturation (SO_2) or the cerebral metabolic rate of oxygen consumption ($CMRO_2$) (Fig.
147 1I,J, K, L). Consistent with our previous findings (Shaw et al., 2021a), flux, HbT and SO_2 were lower in HC
148 than V1, while $CMRO_2$ was the same. Therefore, the decrease in vascular density and increased
149 coefficient of variation in APOE4 mice is not sufficient to drive net alterations in CBF or blood
150 oxygenation, despite the absence of clear compensatory alterations in the diameter, RBC content or
151 flow in individual vessels.

152 We then tested how much the measured vascular densities and blood SO_2 levels might impact on
153 tissue oxygen concentrations, using a simple model of oxygen diffusion into the tissue that we
154 developed previously (Shaw et al., 2021a). Calculating blood oxygen concentrations from our measured
155 SO_2 values, we modelled tissue oxygen levels and oxygen consumption at different distances from
156 blood vessels, based on measured vascular densities in each genotype. Our results indicate that both
157 tissue oxygen concentration and oxygen consumption rates in brain tissue are no different between
158 APOE genotypes in either brain region (Figure 1: Supplementary Figure 1).

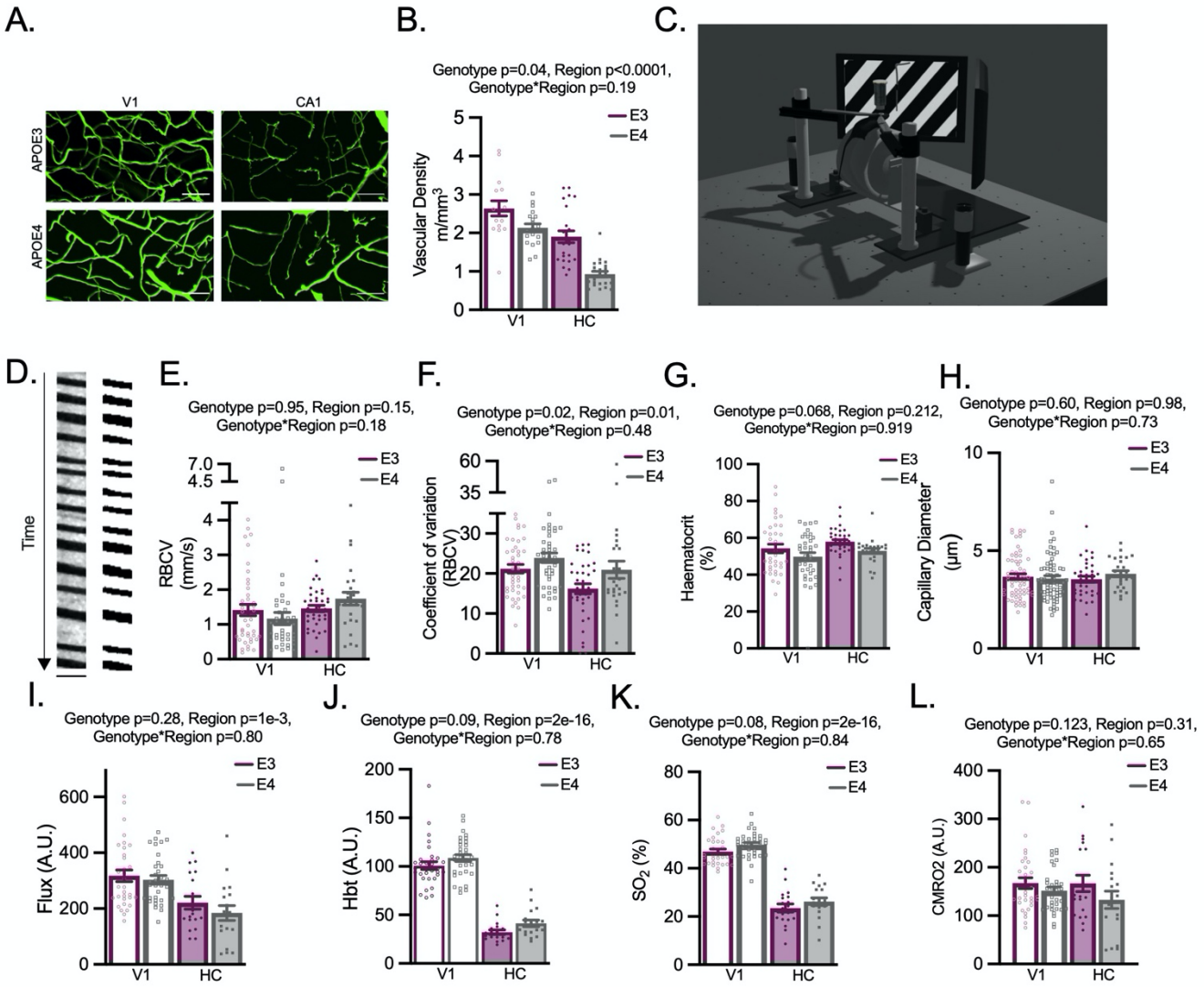

Figure 1. Under baseline conditions functional measurements are largely preserved in APOE4 mice within brain regions, but vascular density is reduced. **A)** Example z-projected images of FITC-gelatin perfused vessels (green). Scale bars: 50 µm. Projected depth: 45.8µm. **B)** Vascular density (of vessels <10 µm in diameter) was reduced in APOE4 animals in V1 and HC. Density was also significantly lower in HC than V1. **C)** Schematic of in vivo imaging set up. Screens display a visual stimulation (drifting grating) as presented to animals with a V1 surgery. Net haemodynamic measurements were recorded using the Oxy-CBF probe and individual vessels and neurons were imaged using 2 photon microscopy. **(D)** Example output from a capillary line scan after preprocessing (left) and the same image binarised (right) for haematocrit measurements. Scale bar (y) = 215ms, (x) = 4.8 µm. No region or genotype differences were found in RBCV **(E)** or in haematocrit **(G)** measures, but RBCV coefficient of variation (CV) was increased in APOE4 animals across regions, and decreased in HC compared to cortex **(F)**. **(H)** No genotype differences were observed in capillary diameters. Regional differences in net measurements of (I) flux**, (J)** HbT and **(K)** SO_2 were observed, with values being lower in HC vs V1. Trend level increases were observed in HbT and SO_2 measures of APOE4 mice. Individual dots on bar plots represent individual slices (B), individual vessels (E-H) and individual recording sessions (I-L). See appendix (i) for sample sizes and details on statistical tests. See also: Figure 1: Supplementary Figure 1

178
179 **Neuronal activity is unchanged at baseline, but APOE4-TR animals display a hyperactive phenotype**
180 **in response to visual stimulation.**
181 To allow us to relate vascular function to neuronal activity – i.e. to study neurovascular coupling – we
182 bred APOE-TR mice with mice expressing GCaMP6f under the control of the Thy1 promoter, to
183 generate mice which expressed GCaMP6f primarily in excitatory neurons (Dana et al., 2014) and were
184 homozygous for APOE3 or APOE4 in place of murine APOE.

185 First, we characterised neuronal activity in the two genotypes. We imaged neuronal calcium activity in
186 V1 and CA1 pyramidal cells (Fig. 2A) during baseline conditions, as well as evoked activity in the visual
187 cortex during presentation of a drifting grating (Fig. 1C). We detected calcium events as peaks in the
188 fluorescence signal in each region of interest (ROI) normalised to baseline (Fig. 2B). We assessed the
189 number and size of individual calcium responses, how correlated cells' firing was across the field of
190 view (FOV) and measured the network response across all cells during visual stimulation. At baseline,
191 neuronal activity was no different between APOE3 and APOE4 mice in either region (correlation, size or
192 frequency of calcium peaks Fig, 2C-E)

193 In contrast, there was a larger change in fluorescence in response to a visual stimulation in APOE4-TR
194 mice (Fig. 2F, G), though the number of cells that significantly increased their calcium during visual
195 stimulation was unchanged (Fig. 2H). Therefore, calcium signals increase more in cells responsive to a
196 visual stimulus in APOE4 compared to APOE3 TR mice. This effect could be due to increased calcium
197 signals to the same level of electrical excitation or increased depolarisation or spiking of these cells
198 during visual stimulation. Both options are plausible: calcium handling has been shown to be impaired
199 in astrocytes of male APOE4-TR mice (Larramona-Arcas et al., 2020), while neurons of old APOE4-TR
200 mice have been shown to be hyperactive due to decreased inhibitory GABAergic tone (Nuriel et al.,
201 2017). We could not test whether a similar enhanced response to stimulation occurs in the HC as
202 neurons are not activatable by a specific "stimulus" in the same way as in V1.

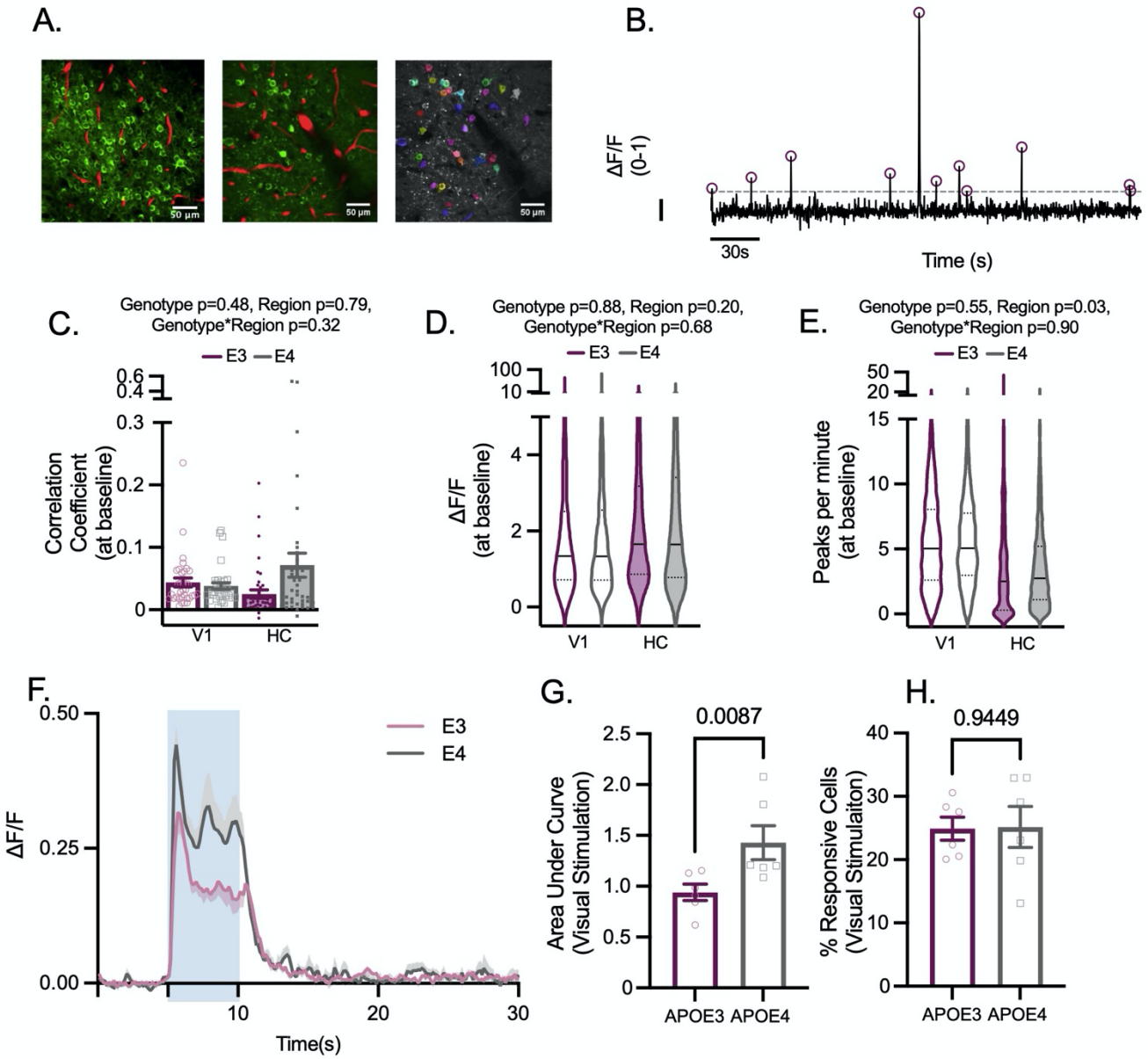

Figure 2. Under baseline conditions, genotypes display the same neuronal characteristics, but during visual stimulation APOE4 animals have larger neuronal responses.(**A)** Left: Thy1-GCaMP expressing neurons (green) and Texas Red filled vasculature (red) from CA1 (left panel) and visual cortex (middle panel). Right panel: ROIs overlying individual cells as detected using Suite2P (Pachitariu et al; 2016). **(B)** Example ΔF/F trace from one ROI, normalised between 0-1. Dashed line depicts threshold for peak selection, circles represent detected peaks and scale bar represents ΔF/F of 0.1 on the y axis and 30 s on the x axis. At baseline, **(C)** the correlation between individual cells within a recording, **(D)** the size of detected peaks per ROI, and **(E)** the number of detected peaks per ROI did not differ between genotypes. There were no regional differences in the correlation between cells or size of detected peaks, but the number of peaks per minute was lower in HC than V1. In visual cortex, the size of the neuronal response to 5s visual stimulation (blue shaded region) was larger in APOE4 animals **(F, G)** but the percentage of neurons that responded to visual stimulation did not differ between genotypes **(H)**. Individual data points plotted in barcharts represent individual fields of view (FOV, C) or animal averages (G,H) and violin plots represent values for individual cells. See appendix (i) for sample sizes and statistical tests.

Vascular responses to visual stimulation are unimpaired in the capillary bed, but pial arterioles are less responsive in neocortex APOE4-TR mice.

Alterations in pericyte function have been previously reported to increase BBB permeability (Bell et al., 2012) and the decreased functional hyperaemia observed in APOE4 mice undergoing acute surgery suggests that the ability of vessels to respond to increased neuronal activity might be altered in APOE4 carriers (Koizumi et al., 2018). We used two separate approaches to study neurovascular coupling in HC and V1, because of different experimental constraints in the two regions. GCaMP6f expression was patchier in V1, so it was not always possible to record calcium signals next to imaged blood vessels, but we could record visual stimulus-evoked responses from the pial arterioles into the capillary bed. However, in HC, whilst we could not measure stimulus-evoked responses, and the large feeding vessels were too deep to be imaged, but we could image capillaries and small arterioles adjacent to spontaneous local neuronal calcium signals.

In V1, we measured vascular diameter changes in response to stimulation in pial arterioles and downstream capillaries, as well as stimulus-evoked changes in RBCV in capillaries. In a healthy system, visual stimulation evokes neuronal activity in the visual cortex and blood flow to the area increases accordingly, seen as increased dilations in capillaries and upstream pial vessels, and an increase in RBCV in individual vessels (Fig. 3E, A, I). The frequency and size of dilations in response to visual stimulation were the same in the capillary bed of APOE3 and APOE4-TR mice (Fig. 3F, G, H). However, the frequency of upstream pial dilations was decreased in APOE4-TR mice, as was the percentage of vessels in which RBCV increased during visual stimulation (Fig. 3D, L). Furthermore, the size of these responses, when they did occur, was no different between genotypes (Fig. 3B, C, J, K), suggesting the potential for dilation remained the same in both genotypes. This was also the case when the size of the pial arteriole response was normalised to the larger neuronal responses in APOE4 vs APOE3 TR mice to generate a neurovascular coupling index (NVCindex; Figure 3: Supplementary Figure 1). Because vasodilation propagates upstream from the capillary bed (Chen et al., 2014; Iadecola et al., 1997), this decreased reliability of APOE4-TR mice pial vessels in the absence of changes in capillary responsiveness may suggest an impairment in the propagation of dilation from the capillaries, rather than in the capacity of pericytes and smooth muscle cells to dilate.

However, these alterations in vascular responsivity did not affect the overall haemodynamic response, with CBF, sO_2 and blood volume (total haemoglobin: HbT) responses to visual stimulation the same across genotypes (Figure 3: Supplementary Figure 2). The neurovascular changes observable at the single vessel level are therefore not, in these conditions, sufficient to affect these macroscopic measurements of functional hyperaemia. The lack of a genotype effect on overall CBF is consistent with the unimpaired capillary responses, as the capillary bed represents the majority of the resistance in the vascular bed, so is expected to mediate most of the increase in CBF during functional hyperaemia (Blinder et al., 2013; Hall et al., 2014), but is different from previous reports in anaesthetised mice showing a substantial reduction in functional hyperaemia to whisker stimulation (Koizumi et al., 2018).

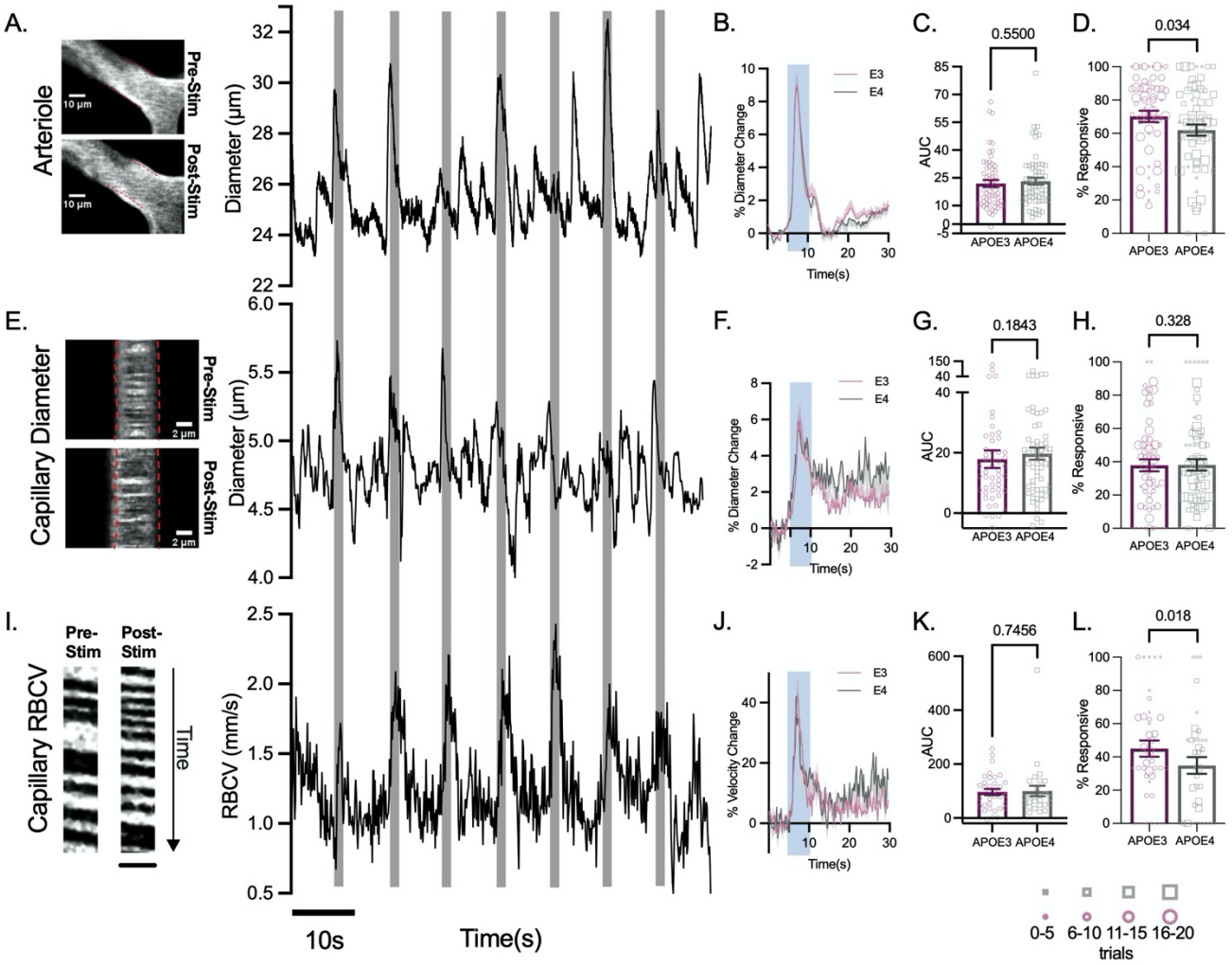

Figure 3. Vascular responses to visual stimulation are less reliable in visual cortex of APOE4 mice, but response sizes do not differ between genotypes. Example images and time series traces of pial arteriole diameter **(A)**, capillary diameter **(E)** and capillary RBCV **(I)** responses to visual stimulation (Scale bar (y) = 260ms, (x) = 5.6 µm). The response magnitude did not differ between genotypes in either the arteriole diameter **(B, C)**, capillary diameter **(F, G)** or capillary RBCV **(J, K)**. In APOE4 mice, the pial arteriole **(D)** and RBCV **(L)** response frequency was reduced, however there was no difference in the frequency of response to visual stimulation in capillary diameters **(H)**. Response frequency was weighted according to the number of contributing trials per vessel. The size of the individual data points reflects the number of trials, as per legend. Individual dots on bar plots represent the data points for individual vessels. See appendix (i) for sample sizes and statistical tests. See also Figure 3: Supplementary Figures 1 and 2.

In the HC, where we could not record from pial vessels but could directly relate local calcium changes to single vessel dilations, we found that while the average responsivity per vessel was not different across genotypes (Fig, 4A), there were more blood vessels that never responded to local calcium events (Fig. 4B), and fewer calcium events resulted in a dilation of local vessels in APOE4 vs APOE3 mice (Fig. 4C), despite similar increases in local neuronal activity (Fig. 4D, E). As in the visual cortex, dilations were not significantly different in size when they did occur (Fig. 4F-H). However, the reduced reliability of vascular responses was not sufficient to reduce the net regional responses to net changes in neuronal activity, as assessed by the size of fluctuations in total haemoglobin, blood flow or sO2 following fluctuations in CMRO2 (Figure 4: Supplementary Figure 1).

These results show that in both HC and V1, neurovascular coupling was mildly disrupted, as blood vessels dilated less frequently to increases in neuronal activity, but that these changes did not affect overall haemodynamics.

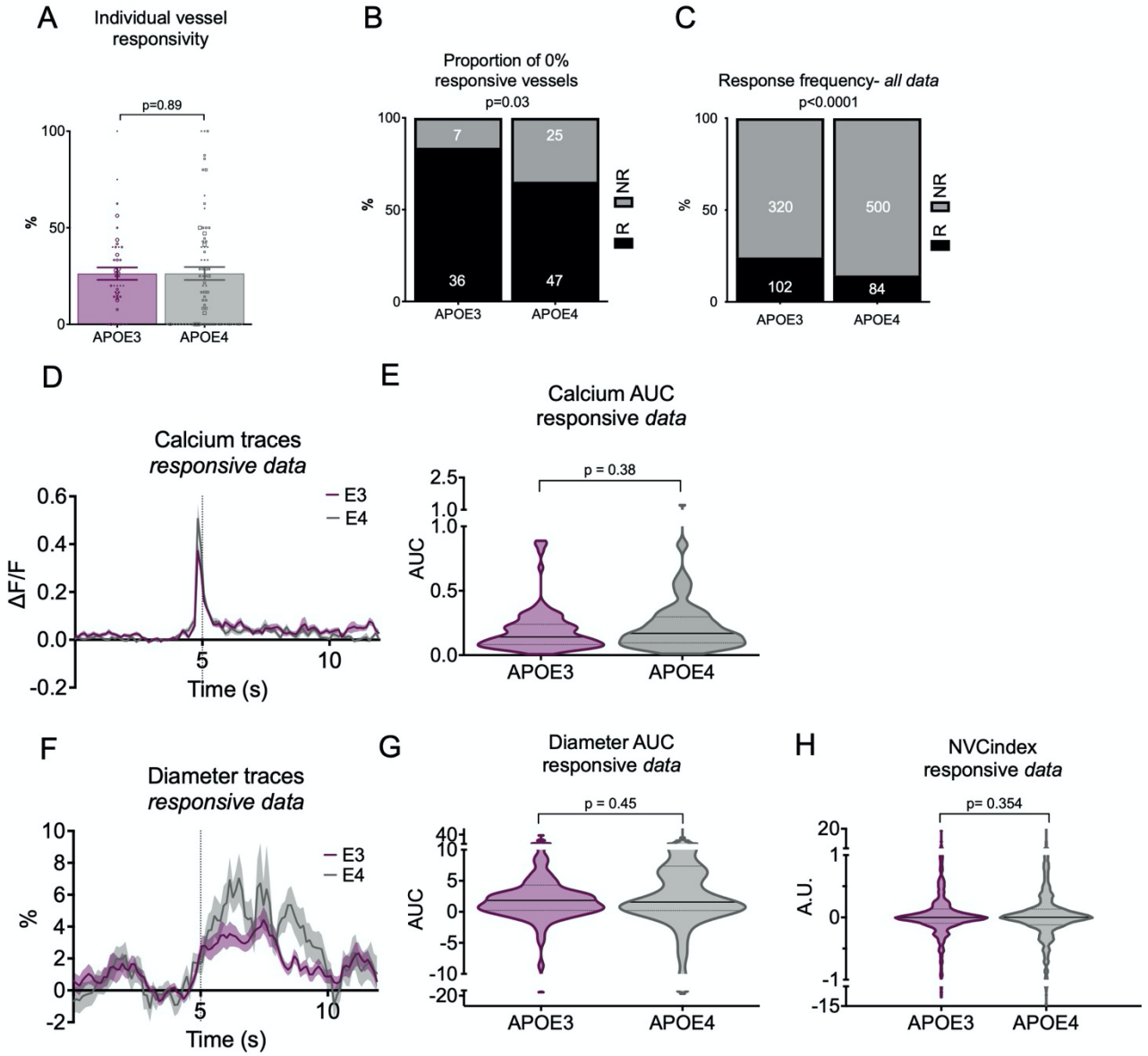

Figure 4. Vascular responses to preceding calcium events are less reliable in CA1 of APOE4 mice, but response sizes do not differ between genotypes. **(A)** Calcium evoked response frequency per individual vessel (for vessels with at least 3 contributing trials) was not different between APOE3 and APOE4 mice when data was weighted according to the number of contributing trials. The size of the individual data points reflects the number of trials, with the smallest dots corresponding with the data with the least trials (*symbol size 1: 3-5 trials, symbol size 2: 6-10 trials, symbol size 3: 11-15 trials, symbol size 4: 16+ trials*). **(B)** Local net calcium events were detected for each recorded vessel, and all recordings with >=3 calcium peaks were retained. Vessel responsiveness to the local net calcium event was classified, and overall response rates (%) were calculated per vessel. Significantly more vessels never responded (0% response rate) to preceding net calcium activity in APOE4 mice compared to APOE3 **(C)** Vessel response frequency to preceding individual calcium events was higher in APOE3 than APOE4 mice. **(D)** calcium peaks and **(F)** diameter traces were plotted for responsive dilations only **(E, G)** The AUC of the **(E)** preceding calcium peaks and vessel peaks **(G)** was not different between genotypes. **(H)** The neurovascular coupling index (dilation peak/calcium peak) was not different between genotypes. The individual values in the bar charts represent individual vessels and for D-H data points represent individual calcium events (and corresponding vascular responses). See appendix (i) for sample sizes and statistical tests. See also Figure 4: Supplementary Figure 1.

305 **APOE4-TR mice have impaired vasomotion.**

306 Arteries and arterioles oscillate at low frequencies (~0.1Hz) — a phenomenon termed vasomotion
307 (Mayhew et al., 1996). In addition to being indicative generally of vascular function and health (Das et
308 al., 2021), vasomotion has also been shown to be one of the drivers of clearance from the brain (van
309 Veluw et al., 2020) and is altered in mouse models of Alzheimer's disease (Di Marco et al., 2015). As
310 AD, and indeed APOE4, is associated with a reduction in clearance of Aβ, we tested whether
311 vasomotion in pial arterioles in V1 (Fig. 5A) was affected by APOE genotype. Fourier transforms of our
312 diameter traces (Fig. 5B) decompose the time course of diameter changes into a spectrum of the
313 power of fluctuations at different frequencies, revealing peaks of increased power at the vasomotion
314 frequency (~0.1Hz) (Fig. 5C). However, the power at this frequency was strikingly lower in APOE4 mice
315 (Fig. 5D), quantified by measuring the power at 0.1Hz (Fig. 5E). This was not because of differences in
316 locomotion during recording (Fig. 5F).

317 It has been demonstrated by others that vasomotion, although an intrinsic vascular property, can be
318 entrained by neuronal activity (Mateo et al., 2017), in particular the gamma band envelope, so we
319 wondered if the decrease in vasomotion could be due altered neuronal activity across the frequency
320 domain. Fourier analyses on GCaMP6f data, though acquired at too low a frequency to directly
321 measure gamma band activity, can nevertheless reveal neuronal oscillatory activity that correlates with
322 vasomotion (He et al., 2018). However, there was not only no peak in the neuronal power spectrum in
323 the vasomotion range (Fig. 5G), but the power also did not differ between genotypes (Fig. 5H). That the
324 APOE4-TR calcium power spectra, though very variable, were not reduced at low frequencies relative
325 to the APOE3 TR signals, suggests that the observed reduction in oscillatory activity in APOE4 mice is
326 likely vascular rather than neuronal in origin, at least as far as can be reflected in excitatory neuronal
327 calcium signals. There were no observed peaks nor significant differences in power across genotypes at
328 the vasomotion frequency in capillary diameters in V1 nor in vessel diameters recorded in CA1 (where
329 we could not image the large feeding arterioles in HC that are equivalent to pial arterioles as these lie
330 beyond our maximum imaging depth ; Figure 5: Supplementary Figure 1), consistent with our previous
331 observations of low vasomotion in these vessels (Shaw et al., 2021b).

332

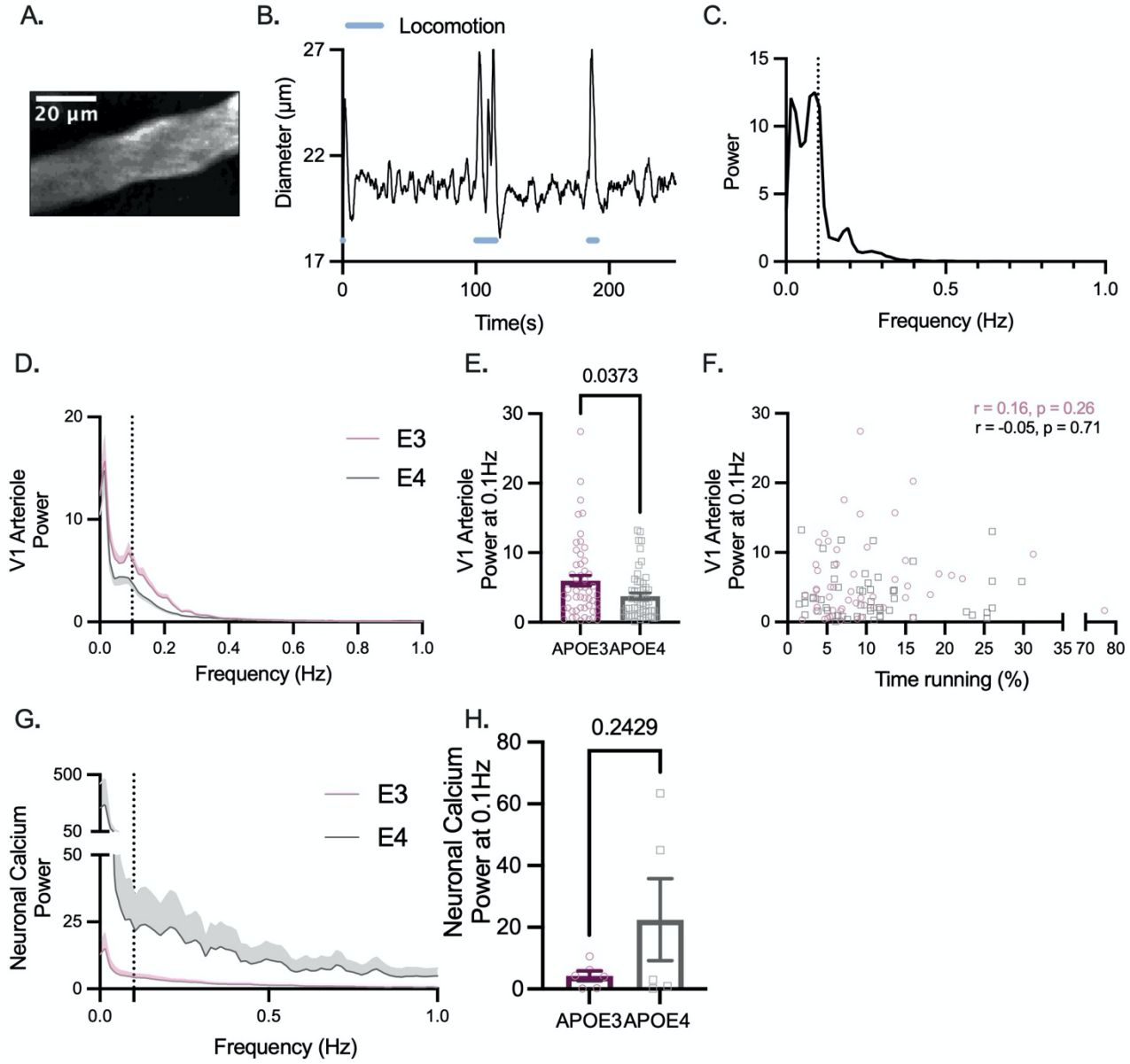

Figure 5. Vasomotion is reduced in the arterioles but not capillaries of APOE4 mice.(**A)** Example 2-photon image showing a representative pial arteriole from V1 (**B)** Example V1 pial arteriole diameter trace showing spontaneous fluctuations in diameter in the absence of locomotion (blue line) or sensory stimulation. **(C)** Power spectrum of diameter trace shown in B. Peak frequency can be observed at ~0.1Hz (dashed line). **(D)** Average power spectra of arteriole diameter traces from APOE3 (pink) and APOE4 (grey) mice. Dashed line at 0.1Hz**. (E)** Arterioles from APOE4 mice have lower power at 0.1Hz**. (F)** The power at 0.1Hz was not affected by the amount of time spent running for either genotype. **(G)** Average power spectra for thy1-GCaMP6f fluorescence traces from V1 in APOE3 and APOE4 animals**. (H)** There was no observed difference in the power at 0.1Hz for neuronal calcium. Individual data points represent values for individual vessels (E-F) or animal averages(H). See appendix (i) for sample sizes and statistical tests. See also Figure 5: Supplementary Figure 1.

346 **Age does not modulate neurovascular alterations in APOE4 animals.**

347 For a subset of experiments in the visual cortex we were able to measure vascular and neuronal
348 reactivity to visual stimulation at older ages, to investigate if increased age affected neurovascular
349 function, as previous work has suggested a decrease in neuronal activity with increased age in APOE4
350 mice (Bell et al., 2012). Due to availability of appropriate GCaMP6f-positive mice, we could only
351 measure neuronal activity at 3-4 and 6-7 months, while vascular features were also measured at 12-13
352 months. The size of the dilations of capillaries and arterioles decreased somewhat across genotypes
353 between 3-4 and 6-7 months, but no consistent age-related decreases were observed up to 12 months
354 (Fig. 6A-F). Where responses were affected by genotype in young animals, the same responses were
355 generally seen in older animals, and no genotype effects emerged in any other metric. Specifically, the
356 response frequency (Fig 6G) and vasomotion (Fig 7A-D) of pial arterioles remained significantly lower in
357 APOE4 mice. Neuronal calcium during visual stimulation and baseline RBCV variability remained
358 enhanced in APOE4-TR mice (Fig. 6J, K; (Figure 6: Supplementary Figure 1)). One measure - the
359 frequency of RBCV increases to visual stimulation - was no longer different between APOE4 and APOE3
360 TR mice (Fig. 6I)) when studied across the whole age range studied, though not because of any
361 significant differences between the ages studied.

362 Together, these data suggest that, rather than declining with age, neurovascular function in APOE3 and
363 APOE4-TR mice is stable, showing specific and persistent differences in pial arteriole responsivity,
364 irregular vasomotion and neuronal function at least until late middle or early old age.

365

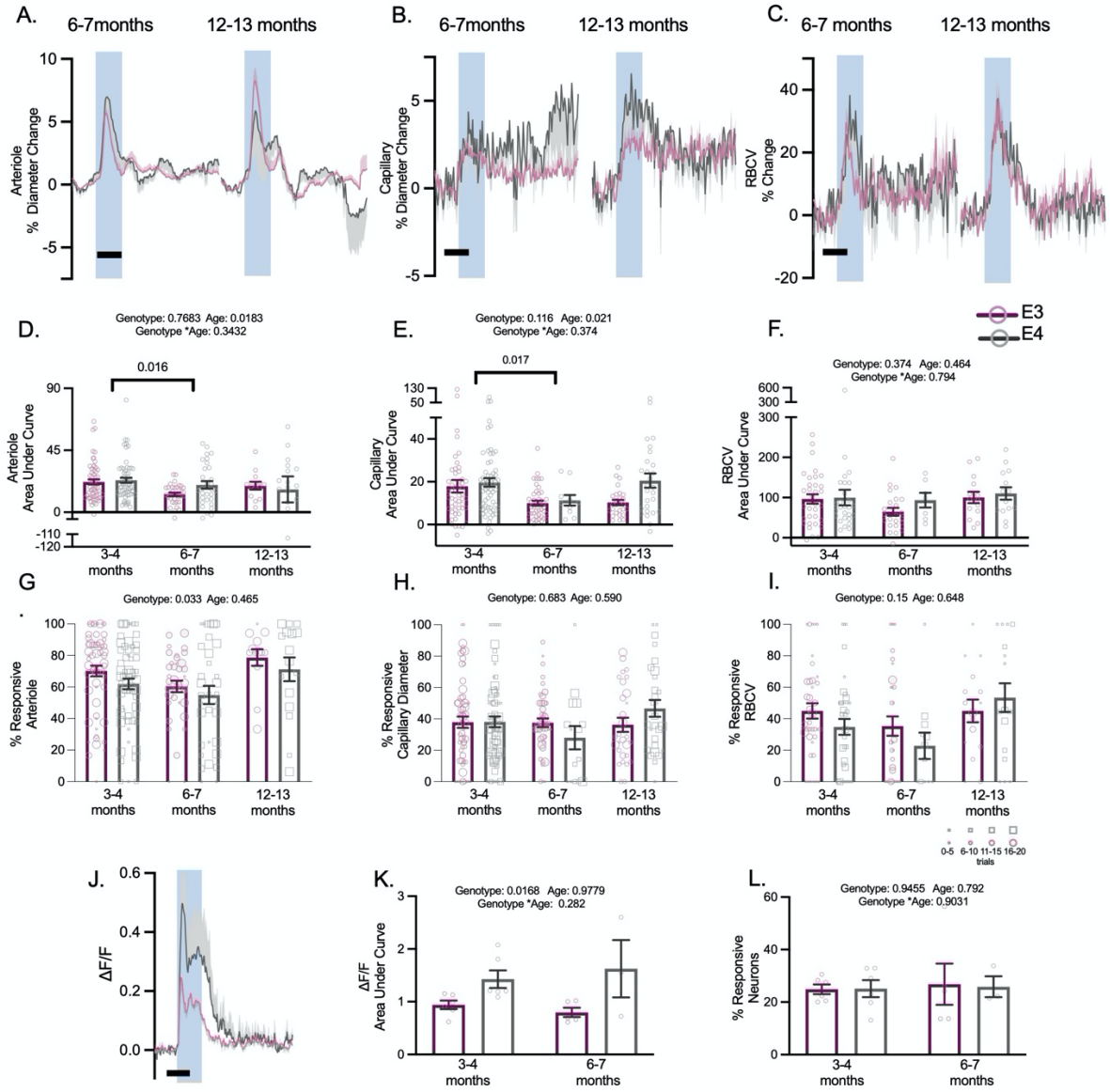

Figure 6. Age does not robustly modulate vascular or neuronal responses to visual stimulation. There was no genotype effect on the response magnitude to visual stimulation in animals across all age points **(A-F)**. In both arteriole diameter and capillary diameter measurements, there was an effect of age, with 3-4 month animals displaying larger responses to stimulation than at 6-7 months, however this effect was not observed in 12-13 month old animals. Response frequency to visual stimulation continued to be modulated by genotype across all ages in arteriole responses to stimulation **(G)**, however they were not affected by age. Neither capillary diameter response frequency **(H)** or RBCV response frequency **(I)** was modulated by age or genotype. At 6-7 months, neuronal responses to stimulation continued to be larger in APOE4 animals **(J, K)**, but this effect was not modulated by age. The response frequency of neurons to stimulation was not affected by age or genotype **(L)**. Individual dots on bar plots represent the values for single vessels (D-I) or animal average (K, L). Response frequency was weighted according to the number of contributing trials per vessel. The size of the individual data points reflects the number of trials, as per legend Scale bars = 5 s. Shaded regions represent the presentation of a visual stimulation. See appendix (i) for sample sizes and statistical tests. See also Figure 6: Supplementary Figure 1.

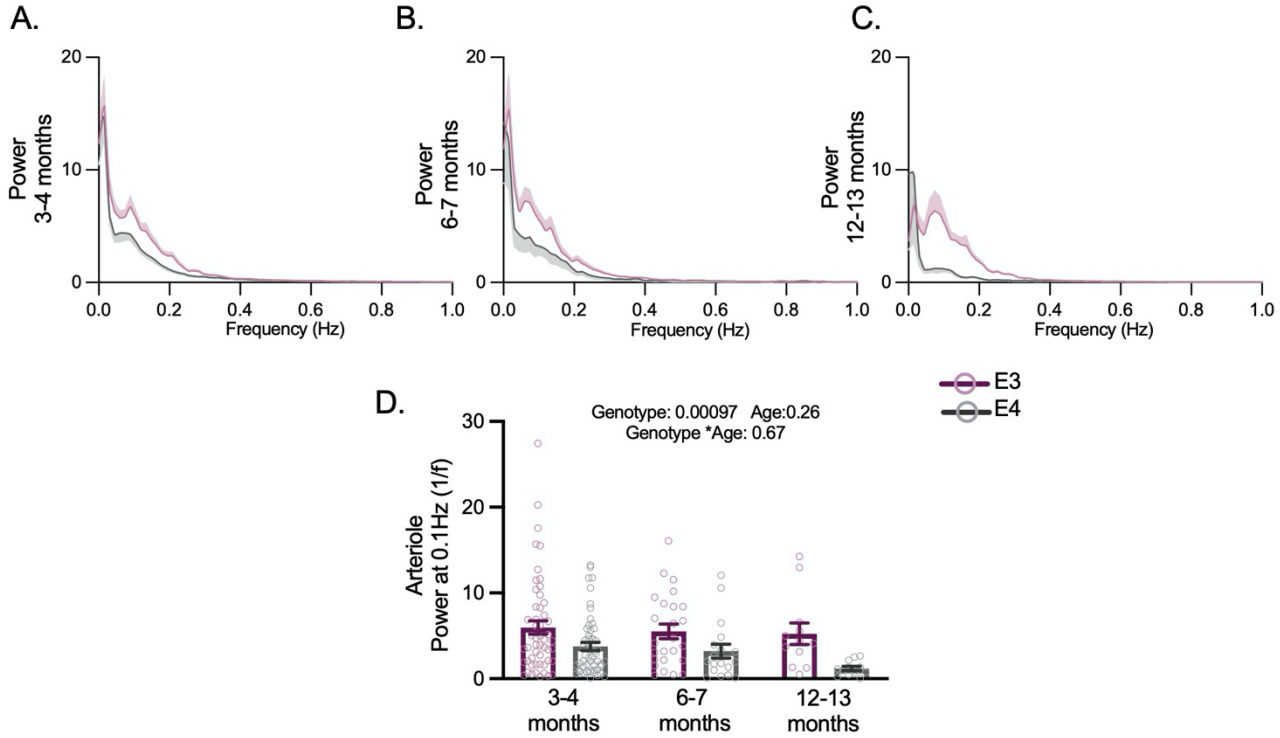

Figure 7. Vasomotion is reduced across all age points but does not appear to be modulated by age. Average power spectra of arteriole diameter traces across all three age points **(A, B, C)**. APOE4 animals had lower power at 0.1Hz **(D)**. Individual dots on bar plots represent the values for single vessels. See appendix (i) for sample sizes and statistical tests.

Discussion

This was the first study to elucidate the effect of APOE genotype on neurovascular function at single neuron and vessel resolution in both the cortex and hippocampus of awake mice. Generally, we found milder effects of APOE4 genotype than has been previously suggested. While vascular density was reduced in APOE4 mice, this did not affect baseline CBF, blood sO_2, or RBCV in single capillaries. Net increases in blood flow, sO_2 or blood volume, or the size of single vessel dilations in response to visual stimulation were also not affected (unlike previously found for somatosensory stimulation (Koizumi et al., 2018). Pial and hippocampal arterioles were, however, less likely to dilate to neuronal activation, and in the cortex showed decreased vasomotion in APOE4 compared to APOE3 TR mice. Furthermore, unlike previously reported overall reductions in neuronal activity (Bell et al., 2012), we found an increase in neuronal calcium signals during visual stimulation. These genotype differences were unaffected by age, suggesting they represent a stable state that does not, itself, cause progressive dysfunction. These effects may, instead, interact with other factors to place the system more at risk of dysfunction when external events do occur (e.g., age, infection).

Differences with previous studies

Previous studies have observed a large decrease in the CBF response to whisker stimulation in APOE4-TR mice (Koizumi et al., 2018), and a decrease in neuronal activity in response to hind limb stimulation, measured with voltage dyes (Bell et al., 2012). Although a regional difference between somatosensory and visual cortex cannot be ruled out, a more likely mechanism is the difference in experimental preparation. In our experiments, animals are imaged while awake and alert, having been allowed to recover from surgery for at least two weeks. The other studies utilised an acute preparation in which the mouse underwent cranial window surgery and was still anaesthetised when neuronal or haemodynamic recordings were undertaken. As human APOE4 carriers are more sensitive to anaesthesia than APOE3 carriers (Cai et al., 2012), mouse models of disease can be more susceptible to cortical spreading depression after invasive surgery (Shabir et al., 2020), and APOE4 is associated with an enhanced inflammatory phenotype (Kloske and Wilcock, 2020), the increased pathology observed in acute preparations may be due to this increased sensitivity to surgery and/or anaesthesia. Our findings, that there is an enhancement of neuronal activity and a slight disruption of vascular function, are a much closer approximation to the mild changes seen in young to middle-aged human APOE4 carriers (Henson et al., 2020; O'Donoghue et al., 2018).

Physiological impact of APOE4 changes in neurovascular function

We initially hypothesised that the mild changes we observed in young animals might progress into worse pathology with age. We wondered if the increased neuronal activity observed in the visual cortex, suggesting an increased energy demand, might be insufficiently provided for by the less responsive vasculature leading to an energy imbalance that could eventually drive neuronal and vascular damage. Our data suggest that this is not the case. The alterations in V1 neuronal and vascular function remained largely stable from 3 to 12-13 months of age. Instead, therefore, our data suggest that APOE4-TR mice are different from APOE3 TR mice in specific, subtle, but consistent ways. This parallels findings in humans of the existence of subtle differences between healthy APOE3 and 4 carriers (higher default mode network functional connectivity in APOE4s), but the lack of age-

442 dependent changes in any measures studied, from cognition to brain structure (Henson et al., 2020) .
443 The genotype differences do not, therefore, cause significant or progressive pathology in healthy,
444 active individuals (our mice are housed in an enriched environment with access to an exercise wheel),
445 but may cause APOE4 carriers (mice or humans) to be more sensitive to triggers that can then cause
446 progression into a pathophysiological state. Such a trigger could be acute surgery under anaesthesia, as
447 discussed above, experimental interventions such as decreased cerebral perfusion (Koizumi et al.,
448 2018), environmental changes such as exposure to infection, a sedentary lifestyle, extreme age or, as in
449 the two-hit hypothesis of AD , factors that initiate the accumulation of Aβ (Zlokovic, 2011).
450
451 A key issue for future research is then to untangle how existing differences between APOE3 and 4
452 carriers interact with additional triggers to cause a change from a stable state to progressive pathology
453 and neurodegeneration. Because cardiovascular risk factors potentiate the risk of someone carrying an
454 APOE4 allele developing AD (Juul Rasmussen et al., 2020), vascular factors are likely involved in this
455 switch, while neuronal changes that could potentiate production of Aβ are also relevant. Some such
456 APOE4-mediated differences are already known, including increased BBB permeability and pericyte
457 inflammation (Bell et al., 2012; Montagne et al., 2020). Our results add three further features for
458 consideration: increased neuronal calcium signals to stimulation, decreased vessel responsivity, and
459 decreased pial vasomotion.
460
461 ***Neuronal calcium:*** Before our study, increased neuronal calcium levels have been previously reported
462 in cultured neurons exposed to ApoE4 both at rest and in response to stimulation (NMDA application,
463 (Qiu et al., 2003); or mechanical injury, (Jiang et al., 2015); though in the latter, ApoE4 had no effect on
464 resting calcium). Whether or not these observations and the increased signals we measure in vivo are
465 due to increased neuronal depolarisation or altered calcium handling (as has been found in APOE4-
466 positive astrocytes from male mice; (Larramona-Arcas et al., 2020)), the ubiquity of the involvement of
467 calcium in cellular processes means that these alterations are likely to be physiologically relevant. The
468 increase in calcium, and its ability to modulate synaptic strengths could therefore potentially underlie
469 the increased connectivity and gamma band oscillations observed in human APOE4 carriers (Henson et
470 al., 2020). It will be of interest to observe how such circuit changes develop in mice, to determine
471 whether this contributes to the decrease in GABAergic inhibitory tone and electrophysiological
472 hyperactivity that develops in old age APOE4 mice (Nuriel et al., 2017). Of particular interest is how
473 these alterations affect how neurons respond to Aβ. Neuronal hyperactivity increases in response to
474 Aβ, but predominantly in cells that are already active (Zott et al., 2019). Therefore, increased neuronal
475 activity caused by ApoE4 may magnify the hyperactivity caused when Aβ is produced, exacerbating its
476 pathophysiological effects.
477
478 ***Vascular responsiveness:*** In our experiments, stimulus evoked pial dilations and calcium dependent
479 dilation of CA1 arterioles and capillaries occur less frequently in APOE4-TR mice. These alterations in
480 pial responsiveness were not sufficient to reduce the overall regional increase in CBF, HbT or oxygen
481 delivery but do indicate something is altered in the pial vasculature of these APOE4-TR mice. Because
482 the capillary bed responses were unchanged in the visual cortex, and the pial and CA1 dilations when
483 they did occur were also of the same size in APOE3 and APOE4-TR mice, the capacity of the smooth
484 muscle cells and pericytes of APOE4-TR mice to dilate may not be impaired, but instead the ability of
485 dilations to spread upstream from the capillary bed to trigger upstream dilations may be reduced. A

future research question would be whether endothelial calcium signals are altered as well as those in neurons, as these signals are involved in propagation of vasodilation via activation of transient receptor potential ankyrin 1 channels (TRPA1; (Thakore et al., 2021)) as well as in activating nitric oxide production, which itself can modulate propagation of vasodilation (Kovacs-Oller et al., 2020) .

Pial arteriole vasomotion: Possibly the most striking difference between APOE3 and APOE4-TR mice was the decrease in low frequency fluctuations of pial arteriole diameter in APOE4 mice - a phenomenon known as vasomotion. The mechanism underlying this reduced vasomotion is unclear, especially as we show that smooth muscle cells can dilate to neuronal activity with similar size responses to visual stimulation in APOE4 mice. Though vasomotion has been found to entrain to neuronal activity (Mateo et al., 2017), we find no evidence of a reduced neuronal drive on vasomotion, though this should be confirmed with electrophysiological measurements of local field potentials, to directly examine the gamma band envelope thought to entrain vasomotion.

Whatever the underlying mechanism, our results suggest another way in which, in APOE4 carriers, a system with reduced vasomotion could be stable, but at risk of decline if Aβ production increases: Vasomotion is known to be important for perivascular clearance of waste molecules, including Aβ, from the brain (Aldea et al., 2019) (van Veluw et al., 2020). APOE4 carriers have an increased Aβ burden both in AD and in cerebral amyloid angiopathy, probably as a result of reduced clearance (Greenberg et al., 2020). Whilst there are several mechanisms that have been shown to contribute to this, including reduced clearance across the BBB (Deane et al., 2008) and reduced degradation (Jiang et al., 2008; Miners et al., 2006), our data and others' showing increased perivascular deposits of exogenously applied Aβ in APOE4 mice (Hawkes et al., 2012) point towards reduced perivascular clearance, due to a decreased driving force from vasomotion, as an additional mechanism. Thus, reduced vasomotion may not matter for the normal physiological functioning of the brain until Aβ production increases and clearance fails, allowing Aβ to accumulate further and exacerbate vascular dysfunction.

Conclusion

Together our data point towards a subtle yet robust effect of APOE4 on the neurovascular system across the lifetime. They indicate APOE4-TR mice have increased neuronal calcium signals in response to sensory stimulation that may contribute to the altered network activity observed in humans and older mice, as well as specific deficits in vascular responsiveness and vasomotion that are not on their own sufficient to alter oxygen delivery or cerebral blood flow in healthy mice. However, the nature of these changes suggests that they may be important features that contribute to the decline of the previously stable system when an additional challenge is encountered, be that further vascular damage, infection or initiation of Aβ accumulation. Investigation of how such factors interact with APOE genotype should therefore be interrogated to understand how APOE4 genotype confers risk of developing AD.

528

529 **Materials and Methods**

530 **Animals**

531 All experimental procedures were approved by the UK Home Office, in accordance with the 1986
532 Animal (Scientific Procedures) Act, under a project licence held by C.H. All experiments were carried
533 out on homozygous APOE3-TR or APOE4-TR mice (Knouff et al., 1999; Sullivan et al., 1997), crossed
534 with animals expressing DsRed under the control of the NG2 promoter (Zhu et al., 2008) or with
535 animals expressing GCaMP6f under the control of the Thy1 promoter. APOE-TR mice were bred from a
536 colony at the University of Sussex derived from founders provided as a kind gift from N. Maeda (UNC
537 School of Medicine, USA). All animals were on a C57BL/6 background. Both male and female mice were
538 used in this study. Mice were between 3-4 months old unless otherwise specified. In ageing
539 experiments, 6-7 month mice were the same as those imaged earlier at 3-4 months, while 12-13
540 month mice were a separate cohort. Animals were housed in a temperature-controlled room with a
541 12-hour light/dark cycle and had free access to food and water.
542

543 **Surgical Preparation**

544 Animals were surgically implanted with a cranial window over the primary visual cortex or the CA1
545 subfield of the hippocampus as previously described (Shaw et al., 2021a). Briefly, animals were
546 anaesthetised with isoflurane (~4% at induction, ~1.5 – 2% maintenance) and body temperature was
547 maintained at 37°C using a homeothermic monitoring system (PhysioSuite, Kent Scientific Corporation).
548 A 3 mm hole was created over the visual cortex or CA1, the dura removed, and for V1 surgery a glass
549 window used to seal the exposed area. For CA1 surgery, ~1.3mm of cortex was aspirated and a custom-
550 made cannula with 3mm glass coverslip was inserted into the craniotomy and then secured in place at
551 the skull surface. Custom-made titanium head bars were fixed to the exposed skull to enable later head
552 fixation. Animals were administered subcutaneous injections of saline 0.9% (400µL), buprenorphine
553 (1.2µg, Vetergesic, Ceva), meloxicam (6.2 µg, Metacam, Boehringer Ingelheim) and dexamethasone (120
554 µg, Dexadreson, MSD Animal Health) at induction, and continued to receive meloxicam (100 µg) in food
555 for three days post-surgery.

556

557 **In vivo experiments**

558 For all in vivo experiments, animals were head-fixed atop a cylindrical treadmill and locomotion was
559 recorded using a rotary encoder (Kuebler). Recordings were made during both 'baseline' conditions,
560 defined as the absence of visual stimulation with the animal free to engage in locomotion and, in animals
561 with a window over V1, during visual stimulation. A drifting grating (315°, 2Hz full screen stimulus, with
562 alternating spatial frequency trials of either 0.04 or 0.2 cycles per degree) was presented for 5 seconds
563 on screens (Asus, ~17cm from mouse), with an interstimulus interval of 20 seconds, allowing for stimulus
564 triggered responses to be measured.

565

566

567

568 *2-photon microscopy*

569 Animals were imaged using a 2-photon microscope (Scientifica) and a mode-locked Ti-sapphire laser
570 (Coherent). Images were acquired using a 20x (XLUMPlanFL N, Olympus) or 16x (LWD, Nikon) water
571 immersion objective from tissue excited at with a laser wavelength of 940nm or 970 nm. The objective
572 was shielded with light occluding tape to minimise light artefacts from visual stimulation. Images were
573 collected using SciScan (Scientifica) software.

574 Prior to imaging, animals were injected with a fluorescent dextran. Those with green fluorescence (i.e.,
575 GCaMP6f) were injected with 100µL 2.5% Texas red (Sigma-Aldrich) either subcutaneously (3 kDa) or
576 intravenously via the tail vein (70 kDa), and those with red fluorescence (i.e., DsRed in vascular mural
577 cells) were injected intravenously with 2.5% fluorescein isothiocyanate-dextran (70 kDa FITC-dextran;
578 Sigma-Aldrich), allowing for visualisation of the vasculature. In visual cortex, pial arterioles were
579 identified by the presence of smooth muscle cells (in NG2-DSred animals), or by their morphology and
580 orientation relative to the large pial veins, as well as their response to visual stimulation. Pial arterioles
581 were then followed with x-y recordings (average pixel size: 0.42 x 0.42 μm^2, imaging speed range 3.8–
582 7.6Hz) made after bifurcations, until the vessels penetrated the parenchyma and therefore could no
583 longer be classed as pial. Penetrating arterioles were followed and branching capillaries were imaged
584 using high speed line scans, to record both diameter and RBCV (average pixel size: 0.19 µm, average
585 number of traversals/second = 1224). In animals positive for GCaMP6f, additional x-y recordings
586 (average pixel size: 1.28 x 1.28 μm^2, imaging speed range 3.8–7.6Hz) were taken from the area proximate
587 to vessel recordings at a depth that allowed for clear visualisation of neuronal cell bodies (layer 2/3 (~z
588 = -150µm)). In CA1, images were taken up to ~500 µm from the surface of the window. Both x-y
589 recordings of neuronal calcium across a large FOV (256 × 256 pixels, speed range 6.10–15.26 Hz, speed
590 average 7.75 Hz, pixel size average 1.80 µm) and smaller FOV recordings allowing for concurrent vascular
591 and local neuronal calcium signals (256 × 256 pixels, speed range 3.05–7.63 Hz, speed average 6.64 Hz;
592 pixel size average 0.23 µm) were obtained. RBCV measurements were obtained as above using high
593 speed linescans (average pixel size: 0.18 µm, average number of traversals/second = 791).

594

595 *Oxy-CBF probe*

596 Regional, or net (~500 um^2) haemodynamic measurements were recorded using a combined laser
597 Doppler flowmetry/ haemoglobin spectroscopy probe (Oxy-CBF probe; Moor Instruments; (Royl et al.,
598 2008) at an acquisition rate of 40 Hz. Net measures of total haemoglobin (HbT), blood flow (flux) and
599 oxygen saturation (sO_2) and cerebral metabolic rate of oxygen consumption ($CMRO_2$ – calculated using
600 equation (i) below) were obtained both at baseline and in V1, during visual stimulation.

601

602 i. $$CMRO_2 = CBF(t) \times \frac{HbR\,(t)}{HbT(t)}$$

603

604 CBF represents cerebral blood flow, t represents time, HbR and HbT represents deoxygenated and total
605 haemoglobin respectively.

606 **In vivo data analysis**

607 *Vascular diameter and RBCV measurements*

608 Prior to analysis, several preprocessing steps were carried out in ImageJ (FIJI) to improve the quality of
609 images as required. Such adjustments included registration, despeckling and/or median 3D filtering. In
610 addition, all images had the 'stack contrast adjustment' plug-in applied to minimise any light artifacts
611 arising from the visual stimulation. A custom MATLAB script was written to analyse vessel diameter using
612 the full width at half maximum (Lab, 2021). Briefly, a skeleton was generated along the centre of each
613 vessel and an intensity profile was plotted along a line perpendicular to the vessel. Values were obtained
614 across a window of five vessel skeleton pixels and averaged to obtain a mean value per window. This
615 was repeated at every second skeleton point, allowing for diameter measurements to be made along
616 the full vascular arbour. These measurements were then averaged along the vessel, resulting in an
617 average diameter per frame.

618 In high speed line scan experiments, similar methods were used to measure the diameter of capillaries
619 imaged using windows of 40ms. Red blood cell velocity measurements were calculated with a radon
620 transform using freely available code (Drew et al., 2010) . In brief, the angle of shadows cast by the RBCs
621 (that do not uptake fluorescent dextran) were measured and used to calculate the velocity across 40ms
622 time windows that overlapped by 10 ms. Angles that were extremely large or small (because of motion
623 artefacts) were removed. To further account for noise in the data obtained from line scans, traces went
624 through either one (diameter) or two (RBCV) iteration(s) of outlier removal. In addition, for stimulation
625 experiments, trials missing greater than 10% of data were excluded and those that remained were
626 subsequently smoothed using a loess smoothing method (range: 1-5% span of the total number of data
627 points, depending on which best represented the shape of the data). To determine AUC measurements,
628 data was interpolated to fill in missing values, using a moving mean average.

629 A coefficient of variation was calculated for RBCV for each individual vessel, to measure temporal
630 variation, by dividing the standard deviation over time by the mean value. To calculate haematocrit,
631 images acquired of shadows cast by RBCs were binarised and the percentage area taken up by RBCs was
632 calculated (black pixels vs. white pixels).

633

634 *Neuronal fluorescence measurements*

635 Regions of interest (ROIs) over individual neurons were identified in GCaMP6f recordings, using the
636 freely available software Suite2p (Pachitariu et al., 2016). A fluorescence signal was extracted from each
637 ROI, along with a background measure (F_{neu}). To reduce out-of-focus neuropil contamination of the
638 signal, 0.7 x F_{neu} was subtracted from each ROI (Chen et al., 2013).

639

640

641

Baseline analysis (no visual stimulation)

Neuronal measures: Baseline measures of neuronal activity were computed in rest (no locomotion) epochs of lasting at least 10 seconds by counting peaks per minute and the size of these peaks. To find peaks in the calcium signal, traces were first scaled so that all values fell between zero and one (equation ii). Peaks during rest periods were identified as being at least twice the standard deviation of the whole trace, and 0.25 seconds apart from the next peak. Each original trace was then normalised as is standard, (equation iii) and the size of each peak was determined and the number of peaks per minute was computed. During rest, the correlation of ROIs within a field of view was measured.

(ii) $\Delta F/F = (F-F_{min})/(F_{max} - F_{min})$

(iii) $\Delta F/F = (F-F_0)/abs(F_0)$

F represents the fluorescence trace. F represents the data trace (fluorescence), and F_0 represents the baseline period to which the rest of the data is normalised.

Haemodynamic measures: For data that were recorded in the absence of a visual stimulation, rest periods were found as above for neuronal activity and an average value per vessel or animal (as specified in individual figure legends) was calculated for each measured parameter.

Detection of hippocampal vessel responses to local calcium events: Peaks in calcium traces were identified as being at least 1.5 times the standard deviation of the whole trace average, and 2 seconds apart from the nearest peak. The corresponding vessel traces (i.e. in the same FOV as neuronal region of interest) were then cut around the same time points. Responsive diameter traces were those where a dilation greater than 1 times the standard deviation of the baseline occurred for more that 0.5 seconds within 5 seconds of the calcium event. Response thresholds were chosen to best separate responses from non-responses.

Visual stimulation data analysis

Neuronal and vessel diameter data acquired from visual stimulation experiments in V1 were cut into trials around the stimulus presentations and averaged to yield a mean response per vessel or animal, as specified in figure legends. Only trials where there was no significant locomotion during the period two seconds prior to stimulation onset or during the stimulation period were used. Significant locomotion was defined as an event that was more than one third of a second in length and/or less than one second apart from adjacent locomotion epochs.

Data were normalised to the 5 s baseline preceding the onset of visual stimulation using equation (iii). To determine if there was a response to stimulation, a threshold was set as twice the standard deviation of this 5 s baseline period. Any response larger than this threshold was deemed 'responsive'. For neuronal data all trials were averaged per cell and if the mean response was larger than the threshold,

680 it was deemed a responsive ROI and subsequently averaged to provide a mean response size per animal.
681 A percentage response rate was also calculated per vessel or animal. For vascular data, these trials were
682 averaged per vessel to provide a 'responsive only' trace. Each vessel had a different number of
683 contributing trials (because mice ran different amounts for each recording) and those with a low number
684 of trials were likely to provide more extreme response frequency values (e.g., 0% or 100%). Therefore,
685 the number of contributing trials per vessel was used to weight data when calculating response
686 frequency. When calculating the size of responses, area under the curve (AUC) measurements were
687 taken during the stimulation period using the inbuilt MATLAB function "trapz" which utilizes trapezoidal
688 numerical integration. In. V1, neurovascular coupling indices (NVCindexndex) were calculated by dividing
689 each vascular AUC by the average neuronal AUC for each genotype (as some mice did not express
690 GCaMP6f in neurons, so calcium data was not available for each mouse). In CA1, where neuronal activity
691 was measured local to the vasculature, the NVCindex was calculated by dividing responding vessel
692 diameter peaks by the corresponding neuronal calcium peaks. Similarly in CA1, net haemodynamic peaks
693 were divided by the corresponding $CMRO_2$ peaks

694

695 *Power spectrum analysis*

696 Welch's power spectral density estimates were computed across all traces (including locomotion
697 epochs) for arteriole diameters, calcium fluorescence traces and capillary diameter traces. All spectra
698 were computed from data recorded in the absence of visual stimulation (except for capillary traces in V1
699 which were collected during visual stimulation, however the expected increase in power as a result is
700 not expected to be near 0.1Hz). All data was detrended by subtracting the baseline (the 8th percentile
701 calculated over 15 second time windows (Grijseels et al., 2021)). Discrete Fourier transforms were then
702 carried out across 60 second time windows using the inbuilt MATLAB function "pwelch". Data below 1
703 Hz was selected and interpolated to the same length using linear interpolation. All data underwent
704 outlier removal based on the value at 0.1Hz (all values greater than 3 standard deviations above the
705 mean were removed). This resulted in the removal of a total of three pial arteriole traces (1 x APOE3, 2
706 x APOE4), two capillary traces in V1 (1 x APOE3 and 1x APOE4), three hippocampal vessel traces
707 (1xAPOE3 and 2 x APOE4), and no calcium traces.

708

709 **Vascular density calculations**

710 APOE-TR mice underwent transcardial perfusion under terminal anaesthesia. Animals were first
711 perfused with 0.1 M phosphate buffered saline (PBS) then 4% paraformaldehyde (PFA) in PBS, and were
712 then perfused with 5% gelatin containing 0.2% FITC-conjugated albumin (at 37 ℃). Following at least 30
713 minutes on ice, brain tissue was then extracted and stored in 4% PFA at 4˚C for 24 hours before being
714 transferred to 30% sucrose in PBS for at least 3 days. Tissue was then sliced at 200µm on a vibratome,
715 and slices were imaged using confocal microscopy (Leica SP8, pixel size: 0.45 – 0.57µm). Vascular density
716 was calculated from the length of vascular skeleton per unit volume, using the "Analyse Skeleton" plugin
717 in FIJI/ImageJ (Arganda-Carreras et al., 2010) .

718

Oxygen Modelling

Oxygen modelling was carried out as described previously (Shaw et al., 2021a). Briefly, median and upper lower 95th centile sO2 measurements were used to calculate the pO2 in red blood cells, using the Hill constant for oxygen dissociation from haemoglobin in C57/BL6 cells (Uchida et al., 1998). The plasma pO2 was then estimated from comparison with similar measurements of intra- and interRBC pO2 to determine the capillary pO2(Lyons et al., 2016; Parpaleix et al., 2013). Distance maps were then calculated of 3D stacks of the vasculature of APOE3 and 4 visual cortex and hippocampus, coding every voxel in terms of the distance to the nearest vascular voxel. The median and 95th centile spacing of voxels were calculated from the distribution of these values. Oxygen diffusion across these distances was then modelled by numerically solving Fick's diffusion equation (iv) for radial geometries using the Partial Differential Equation toolbox in MATLAB, with a diffusion coefficient (D) of 9.24 x 10^{-8} m^2/min in brain tissue at 37 °C (Ganfield et al., 1970)and 40% lower in a 200 nm vessel wall surrounding the capillary(Thomsen et al., 2017). Oxygen consumption by the tissue was assumed to follow Michaelis-Menten kinetics with a K_m of 1 μM, from the EC50 for oxygen at cytochrome c oxidase (Cooper, 2003), and a V_{max} of 2 mM/min (Gould et al., 2017).

(iv) $$\frac{dC}{dt} = \frac{1}{r}\frac{d}{dr}\left(rD\frac{dC}{dr}\right) - \frac{V_{max}C}{C+K_m}$$

Statistics

Statistical analyses were conducted in GraphPad Prism 8, SPSS, RStudio or MATLAB. Data are presented as mean +/- SEM except for violin plots where horizonal lines represent the median and interquartile range. Individual data points represent individual blood vessels, brain slices, imaging sessions or animals as specified in figure legends. Where relevant, data whose residuals were normally distributed, as determined by a D'Agostino-Pearson and Shapiro-Wilk test, were compared using an unpaired t test, with a Welch's correction applied if variances were unequal as determined by an F test. Data that were not normally distributed were compared using a non-parametric Mann-Whitney U test. Linear mixed models (LMM) were carried out using 'lmer' in RStudio, with random effects specified in appendix (i). For correlation analyses non-normal data were analysed using Spearman's rank correlation. To weight response frequency data, so that vessels with a larger number of contributing trials contributed more to the mean, a weighted least squares linear regression was used and the mean was weighted by the number of contributing trials. P values below 0.05 were considered significant and those below 0.1 as trending towards significance.

Funding: This work was funded by an Alzheimer's Society DTC PhD studentship to O.B., Sussex Neuroscience PhD studentships for D.G. and D.C., the MRC (MR/S026495/1; MC_PC_15071) and an Academy of Medical Sciences/Wellcome Trust Springboard award to C.N.H.

Acknowledgements:
We would like to thank Jason Berwick and Jimena Berni for helpful discussions on this work.

Author Contributions:

O.B., K.S. and L.B. collected data for the studies. O.B., K.S., S.K. and C.N.H. designed the studies, and O.B., K.S., S.A. and C.N.H. analysed the studies. O.B, K.S, D.M.G, D.C and C.N.H. wrote scripts to analyse the data. O.B. and C.N.H. wrote the manuscript with feedback from all authors.

References

Aldea, R., Weller, R.O., Wilcock, D.M., Carare, R.O., Richardson, G., 2019. Cerebrovascular smooth muscle cells as the drivers of intramural periarterial drainage of the brain. Front. Aging Neurosci. 11, 1. doi:10.3389/fnagi.2019.00001

Angleys, H., Østergaard, L., Jespersen, S.N., 2015. The effects of capillary transit time heterogeneity (CTH) on brain oxygenation. J. Cereb. Blood Flow Metab. 35, 806–817. doi:10.1038/jcbfm.2014.254

Arganda-Carreras, I., Fernández-González, R., Muñoz-Barrutia, A., Ortiz-De-Solorzano, C., 2010. 3D reconstruction of histological sections: Application to mammary gland tissue. Microsc. Res. Tech. 73, 1019–1029. doi:10.1002/jemt.20829

Bell, R.D., Winkler, E.A., Singh, I., Sagare, A.P., Deane, R., Wu, Z., Holtzman, D.M., Betsholtz, C., Armulik, A., Sallstrom, J., Berk, B.C., Zlokovic, B.V., 2012. Apolipoprotein E controls cerebrovascular integrity via cyclophilin A. Nature 485, 512–516. doi:10.1038/nature11087

Blinder, P., Tsai, P.S., Kaufhold, J.P., Knutsen, P.M., Suhl, H., Kleinfeld, D., 2013. The cortical angiome: an interconnected vascular network with noncolumnar patterns of blood flow. Nat. Neurosci. 16, 889–897. doi:10.1038/nn.3426

Browndyke, J.N., Wright, M.C., Yang, R., Syed, A., Park, J., Hall, A., Martucci, K., Devinney, M.J., Shaw, L., Waligorska, T., Moretti, E.W., Whitson, H.E., Cohen, H.J., Mathew, J.P., Berger, M., MADCO-PC Investigators, 2021. Perioperative neurocognitive and functional neuroimaging trajectories in older APOE4 carriers compared with non-carriers: secondary analysis of a prospective cohort study. Br. J. Anaesth. 127, 917–928. doi:10.1016/j.bja.2021.08.012

Cai, Y., Hu, H., Liu, P., Feng, G., Dong, W., Yu, B., Zhu, Y., Song, J., Zhao, M., 2012. Association between the apolipoprotein E4 and postoperative cognitive dysfunction in elderly patients undergoing intravenous anesthesia and inhalation anesthesia. Anesthesiology 116, 84–93. doi:10.1097/ALN.0b013e31823da7a2

Chen, B.R., Kozberg, M.G., Bouchard, M.B., Shaik, M.A., Hillman, E.M.C., 2014. A critical role for the vascular endothelium in functional neurovascular coupling in the brain. J. Am. Heart Assoc. 3, e000787. doi:10.1161/JAHA.114.000787

Chen, T.-W., Wardill, T.J., Sun, Y., Pulver, S.R., Renninger, S.L., Baohan, A., Schreiter, E.R., Kerr, R.A., Orger, M.B., Jayaraman, V., Looger, L.L., Svoboda, K., Kim, D.S., 2013. Ultrasensitive fluorescent proteins for imaging neuronal activity. Nature 499, 295–300. doi:10.1038/nature12354

Cooper, C.E., 2003. Competitive, reversible, physiological? Inhibition of mitochondrial cytochrome oxidase by nitric oxide. IUBMB Life 55, 591–597. doi:10.1080/15216540310001628663

Corder, E.H., Saunders, A.M., Strittmatter, W.J., Schmechel, D.E., Gaskell, P.C., Small, G.W., Roses, A.D., Haines, J.L., Pericak-Vance, M.A., 1993. Gene dose of apolipoprotein E type 4 allele and the risk of Alzheimer's disease in late onset families. Science 261, 921–923. doi:10.1126/science.8346443

Cumming, G., Finch, S., 2005. Inference by eye: confidence intervals and how to read pictures of data. Am. Psychol. 60, 170–180. doi:10.1037/0003-066X.60.2.170

804 Dana, H., Chen, T.-W., Hu, A., Shields, B.C., Guo, C., Looger, L.L., Kim, D.S., Svoboda, K., 2014.
805 Thy1-GCaMP6 transgenic mice for neuronal population imaging in vivo. PLoS One 9, e108697.
806 doi:10.1371/journal.pone.0108697
807 Das, A., Murphy, K., Drew, P.J., 2021. Rude mechanicals in brain haemodynamics: non-neural actors
808 that influence blood flow. Philos. Trans. R. Soc. Lond. B, Biol. Sci. 376, 20190635.
809 doi:10.1098/rstb.2019.0635
810 Deane, R., Sagare, A., Hamm, K., Parisi, M., Lane, S., Finn, M.B., Holtzman, D.M., Zlokovic, B.V.,
811 2008. apoE isoform – specific disruption of amyloid β peptide clearance from mouse brain. J.
812 Clin. Invest. 118, 4002–4013.
813 Di Marco, L.Y., Farkas, E., Martin, C., Venneri, A., Frangi, A.F., 2015. Is vasomotion in cerebral
814 arteries impaired in alzheimer's disease? J. Alzheimers Dis. 46, 35–53. doi:10.3233/JAD-142976
815 Drew, P.J., Blinder, P., Cauwenberghs, G., Shih, A.Y., Kleinfeld, D., 2010. Rapid determination of
816 particle velocity from space-time images using the Radon transform. J. Comput. Neurosci. 29, 5–
817 11. doi:10.1007/s10827-009-0159-1
818 Ganfield, R.A., Nair, P., Whalen, W.J., 1970. Mass transfer, storage, and utilization of O2 in cat cerebral
819 cortex. Am. J. Physiol. 219, 814–821. doi:10.1152/ajplegacy.1970.219.3.814
820 Gould, I.G., Tsai, P., Kleinfeld, D., Linninger, A., 2017. The capillary bed offers the largest
821 hemodynamic resistance to the cortical blood supply. J. Cereb. Blood Flow Metab. 37, 52–68.
822 doi:10.1177/0271678X16671146
823 Greenberg, S.M., Bacskai, B.J., Hernandez-Guillamon, M., Pruzin, J., Sperling, R., van Veluw, S.J.,
824 2020. Cerebral amyloid angiopathy and Alzheimer disease - one peptide, two pathways. Nat.
825 Rev. Neurol. 16, 30–42. doi:10.1038/s41582-019-0281-2
826 Grijseels, D.M., Shaw, K., Barry, C., Hall, C.N., 2021. Choice of method of place cell classification
827 determines the population of cells identified. BioRxiv. doi:10.1101/2021.02.26.433025
828 Hall, C.N., Reynell, C., Gesslein, B., Hamilton, N.B., Mishra, A., Sutherland, B.A., O'Farrell, F.M.,
829 Buchan, A.M., Lauritzen, M., Attwell, D., 2014. Capillary pericytes regulate cerebral blood flow
830 in health and disease. Nature 508, 55–60. doi:10.1038/nature13165
831 Halliday, M.R., Rege, S.V., Ma, Q., Zhao, Z., Miller, C.A., Winkler, E.A., Zlokovic, B.V., 2016.
832 Accelerated pericyte degeneration and blood-brain barrier breakdown in apolipoprotein E4
833 carriers with Alzheimer's disease. J. Cereb. Blood Flow Metab. 36, 216–227.
834 doi:10.1038/jcbfm.2015.44
835 Hamilton, N.B., Attwell, D., Hall, C.N., 2010. Pericyte-mediated regulation of capillary diameter: a
836 component of neurovascular coupling in health and disease. Front. Neuroenergetics 2.
837 doi:10.3389/fnene.2010.00005
838 Hawkes, C.A., Sullivan, P.M., Hands, S., Weller, R.O., Nicoll, J.A.R., Carare, R.O., 2012. Disruption of
839 arterial perivascular drainage of amyloid-β from the brains of mice expressing the human APOE
840 ε4 allele. PLoS One 7, e41636. doi:10.1371/journal.pone.0041636
841 He, Y., Wang, M., Chen, X., Pohmann, R., Polimeni, J.R., Scheffler, K., Rosen, B.R., Kleinfeld, D., Yu,
842 X., 2018. Ultra-Slow Single-Vessel BOLD and CBV-Based fMRI Spatiotemporal Dynamics and
843 Their Correlation with Neuronal Intracellular Calcium Signals. Neuron 97, 925–939.e5.
844 doi:10.1016/j.neuron.2018.01.025
845 Henneman, W.J.P., Sluimer, J.D., Barnes, J., van der Flier, W.M., Sluimer, I.C., Fox, N.C., Scheltens,
846 P., Vrenken, H., Barkhof, F., 2009. Hippocampal atrophy rates in Alzheimer disease: added
847 value over whole brain volume measures. Neurology 72, 999–1007.
848 doi:10.1212/01.wnl.0000344568.09360.31
849 Henson, R.N., Suri, S., Knights, E., Rowe, J.B., Kievit, R.A., Lyall, D.M., Chan, D., Eising, E., Fisher,

S.E., 2020. Effect of apolipoprotein E polymorphism on cognition and brain in the Cambridge Centre for Ageing and Neuroscience cohort. Brain Neurosci. Adv. 4, 2398212820961704. doi:10.1177/2398212820961704

Iadecola, C., 2017. The Neurovascular Unit Coming of Age: A Journey through Neurovascular Coupling in Health and Disease. Neuron 96, 17–42. doi:10.1016/j.neuron.2017.07.030

Iadecola, C., Yang, G., Ebner, T.J., Chen, G., 1997. Local and propagated vascular responses evoked by focal synaptic activity in cerebellar cortex. J. Neurophysiol. 78, 651–659. doi:10.1152/jn.1997.78.2.651

Iturria-Medina, Y., Sotero, R.C., Toussaint, P.J., Mateos-Pérez, J.M., Evans, A.C., Alzheimer's Disease Neuroimaging Initiative, 2016. Early role of vascular dysregulation on late-onset Alzheimer's disease based on multifactorial data-driven analysis. Nat. Commun. 7, 11934. doi:10.1038/ncomms11934

Jiang, L., Zhong, J., Dou, X., Cheng, C., Huang, Z., Sun, X., 2015. Effects of ApoE on intracellular calcium levels and apoptosis of neurons after mechanical injury. Neuroscience 301, 375–383. doi:10.1016/j.neuroscience.2015.06.005

Jiang, Q., Lee, C.Y.D., Mandrekar, S., Wilkinson, B., Cramer, P., Zelcer, N., Mann, K., Lamb, B., Willson, T.M., Collins, J.L., Richardson, J.C., Smith, J.D., Comery, T.A., Riddell, D., Holtzman, D.M., Tontonoz, P., Landreth, G.E., 2008. ApoE promotes the proteolytic degradation of Abeta. Neuron 58, 681–693. doi:10.1016/j.neuron.2008.04.010

Juul Rasmussen, I., Rasmussen, K.L., Nordestgaard, B.G., Tybjærg-Hansen, A., Frikke-Schmidt, R., 2020. Impact of cardiovascular risk factors and genetics on 10-year absolute risk of dementia: risk charts for targeted prevention. Eur. Heart J. 41, 4024–4033. doi:10.1093/eurheartj/ehaa695

Kisler, K., Nelson, A.R., Montagne, A., Zlokovic, B.V., 2017. Cerebral blood flow regulation and neurovascular dysfunction in Alzheimer disease. Nat. Rev. Neurosci. 18, 419–434. doi:10.1038/nrn.2017.48

Kloske, C.M., Wilcock, D.M., 2020. The important interface between apolipoprotein E and neuroinflammation in alzheimer's disease. Front. Immunol. 11, 754. doi:10.3389/fimmu.2020.00754

Knouff, C., Hinsdale, M.E., Mezdour, H., Altenburg, M.K., Watanabe, M., Quarfordt, S.H., Sullivan, P.M., Maeda, N., 1999. Apo E structure determines VLDL clearance and atherosclerosis risk in mice. J. Clin. Invest. 103, 1579–1586. doi:10.1172/JCI6172

Koizumi, K., Hattori, Y., Ahn, S.J., Buendia, I., Ciacciarelli, A., Uekawa, K., Wang, G., Hiller, A., Zhao, L., Voss, H.U., Paul, S.M., Schaffer, C., Park, L., Iadecola, C., 2018. Apoε4 disrupts neurovascular regulation and undermines white matter integrity and cognitive function. Nat. Commun. 9, 3816. doi:10.1038/s41467-018-06301-2

Kovacs-Oller, T., Ivanova, E., Bianchimano, P., Sagdullaev, B.T., 2020. The pericyte connectome: spatial precision of neurovascular coupling is driven by selective connectivity maps of pericytes and endothelial cells and is disrupted in diabetes. Cell Discov. 6, 39. doi:10.1038/s41421-020-0180-0

Lab, B.E., 2021. BrainEnergyLab/HCvsV1_NVC_Manuscript: NVCinHCmanuscript_March2021_release1. Zenodo. doi:10.5281/zenodo.4593010

Larramona-Arcas, R., González-Arias, C., Perea, G., Gutiérrez, A., Vitorica, J., García-Barrera, T., Gómez-Ariza, J.L., Pascua-Maestro, R., Ganfornina, M.D., Kara, E., Hudry, E., Martinez-Vicente, M., Vila, M., Galea, E., Masgrau, R., 2020. Sex-dependent calcium hyperactivity due to lysosomal-related dysfunction in astrocytes from APOE4 versus APOE3 gene targeted replacement mice. Mol. Neurodegener. 15, 35. doi:10.1186/s13024-020-00382-8

896 Lyons, D.G., Parpaleix, A., Roche, M., Charpak, S., 2016. Mapping oxygen concentration in the awake
897 mouse brain. Elife 5. doi:10.7554/eLife.12024
898 Mateo, C., Knutsen, P.M., Tsai, P.S., Shih, A.Y., Kleinfeld, D., 2017. Entrainment of Arteriole
899 Vasomotor Fluctuations by Neural Activity Is a Basis of Blood-Oxygenation-Level-Dependent
900 "Resting-State" Connectivity. Neuron 96, 936–948.e3. doi:10.1016/j.neuron.2017.10.012
901 Mayhew, J.E., Askew, S., Zheng, Y., Porrill, J., Westby, G.W., Redgrave, P., Rector, D.M., Harper,
902 R.M., 1996. Cerebral vasomotion: a 0.1-Hz oscillation in reflected light imaging of neural
903 activity. Neuroimage 4, 183–193. doi:10.1006/nimg.1996.0069
904 Michaelis, E.K., 2012. Selective neuronal vulnerability in the hippocampus: relationship to neurological
905 diseases and mechanisms for differential sensitivity of neurons to stress, in: Bartsch, T. (Ed.),
906 The Clinical Neurobiology of the Hippocampus: An Integrative View. Oxford University Press,
907 pp. 54–76. doi:10.1093/acprof:oso/9780199592388.003.0004
908 Miners, J.S., Van Helmond, Z., Chalmers, K., Wilcock, G., Love, S., Kehoe, P.G., 2006. Decreased
909 expression and activity of neprilysin in Alzheimer disease are associated with cerebral amyloid
910 angiopathy. J. Neuropathol. Exp. Neurol. 65, 1012–1021.
911 doi:10.1097/01.jnen.0000240463.87886.9a
912 Montagne, A., Nation, D.A., Sagare, A.P., Barisano, G., Sweeney, M.D., Chakhoyan, A., Pachicano, M.,
913 Joe, E., Nelson, A.R., D'Orazio, L.M., Buennagel, D.P., Harrington, M.G., Benzinger, T.L.S.,
914 Fagan, A.M., Ringman, J.M., Schneider, L.S., Morris, J.C., Reiman, E.M., Caselli, R.J., Chui,
915 H.C., Tcw, J., Chen, Y., Pa, J., Conti, P.S., Law, M., Toga, A.W., Zlokovic, B.V., 2020. APOE4
916 leads to blood-brain barrier dysfunction predicting cognitive decline. Nature 581, 71–76.
917 doi:10.1038/s41586-020-2247-3
918 Najm, R., Jones, E.A., Huang, Y., 2019. Apolipoprotein E4, inhibitory network dysfunction, and
919 Alzheimer's disease. Mol. Neurodegener. 14, 24. doi:10.1186/s13024-019-0324-6
920 Nuriel, T., Angulo, S.L., Khan, U., Ashok, A., Chen, Q., Figueroa, H.Y., Emrani, S., Liu, L., Herman,
921 M., Barrett, G., Savage, V., Buitrago, L., Cepeda-Prado, E., Fung, C., Goldberg, E., Gross, S.S.,
922 Hussaini, S.A., Moreno, H., Small, S.A., Duff, K.E., 2017. Neuronal hyperactivity due to loss of
923 inhibitory tone in APOE4 mice lacking Alzheimer's disease-like pathology. Nat. Commun. 8,
924 1464. doi:10.1038/s41467-017-01444-0
925 O'Donoghue, M.C., Murphy, S.E., Zamboni, G., Nobre, A.C., Mackay, C.E., 2018. APOE genotype and
926 cognition in healthy individuals at risk of Alzheimer's disease: A review. Cortex 104, 103–123.
927 doi:10.1016/j.cortex.2018.03.025
928 Pachitariu, M., Stringer, C., Schröder, S., Dipoppa, M., Rossi, L.F., Carandini, M., Harris, K.D., 2016.
929 Suite2p: beyond 10,000 neurons with standard two-photon microscopy. BioRxiv.
930 doi:10.1101/061507
931 Parpaleix, A., Goulam Houssen, Y., Charpak, S., 2013. Imaging local neuronal activity by monitoring
932 PO_2 transients in capillaries. Nat. Med. 19, 241–246. doi:10.1038/nm.3059
933 Qiu, Z., Crutcher, K.A., Hyman, B.T., Rebeck, G.W., 2003. ApoE isoforms affect neuronal N-methyl-
934 D-aspartate calcium responses and toxicity via receptor-mediated processes. Neuroscience 122,
935 291–303. doi:10.1016/j.neuroscience.2003.08.017
936 Royl, G., Füchtemeier, M., Leithner, C., Megow, D., Offenhauser, N., Steinbrink, J., Kohl-Bareis, M.,
937 Dirnagl, U., Lindauer, U., 2008. Hypothermia effects on neurovascular coupling and cerebral
938 metabolic rate of oxygen. Neuroimage 40, 1523–1532. doi:10.1016/j.neuroimage.2008.01.041
939 Schenning, K.J., Murchison, C.F., Mattek, N.C., Silbert, L.C., Kaye, J.A., Quinn, J.F., 2016. Surgery is
940 associated with ventricular enlargement as well as cognitive and functional decline. Alzheimers
941 Dement. 12, 590–597. doi:10.1016/j.jalz.2015.10.004

942 Shabir, O., Pendry, B., Lee, L., Eyre, B., Sharp, P., Rebollar, M.A., Howarth, C., Heath, P.R., Wharton,
943 S.B., Francis, S.E., Berwick, J., 2020. Assessment of neurovascular coupling & cortical
944 spreading depression in mixed models of atherosclerosis & alzheimer's disease. BioRxiv.
945 doi:10.1101/2020.08.13.249987
946 Shaw, K, Bell, L., Boyd, K., Grijseels, D.M., Clarke, D., Bonnar, O., Crombag, H.S., Hall, C.N., 2021a.
947 Neurovascular coupling and oxygenation are decreased in hippocampus compared to neocortex
948 because of microvascular differences. Nat. Commun. 12, 3190. doi:10.1038/s41467-021-23508-y
949 Shaw, Kira, Boyd, K., Anderle, S., Hammond-Haley, M., Amin, D., Bonnar, O., Hall, C.N., 2021b.
950 Gradual not sudden change: multiple sites of functional transition across the microvascular bed.
951 Front. Aging Neurosci. 13, 779823. doi:10.3389/fnagi.2021.779823
952 Sullivan, P.M., Mezdour, H., Aratani, Y., Knouff, C., Najib, J., Reddick, R.L., Quarfordt, S.H., Maeda,
953 N., 1997. Targeted replacement of the mouse apolipoprotein E gene with the common human
954 APOE3 allele enhances diet-induced hypercholesterolemia and atherosclerosis. J. Biol. Chem.
955 272, 17972–17980. doi:10.1074/jbc.272.29.17972
956 Sun, X., He, G., Qing, H., Zhou, W., Dobie, F., Cai, F., Staufenbiel, M., Huang, L.E., Song, W., 2006.
957 Hypoxia facilitates Alzheimer's disease pathogenesis by up-regulating BACE1 gene expression.
958 Proc. Natl. Acad. Sci. USA 103, 18727–18732. doi:10.1073/pnas.0606298103
959 Thakore, P., Alvarado, M.G., Ali, S., Mughal, A., Pires, P.W., Yamasaki, E., Pritchard, H.A., Isakson,
960 B.E., Tran, C.H.T., Earley, S., 2021. Brain endothelial cell TRPA1 channels initiate
961 neurovascular coupling. Elife 10, e63040. doi:10.7554/eLife.63040
962 Thambisetty, M., Beason-Held, L., An, Y., Kraut, M.A., Resnick, S.M., 2010. APOE epsilon4 genotype
963 and longitudinal changes in cerebral blood flow in normal aging. Arch. Neurol. 67, 93–98.
964 doi:10.1001/archneurol.2009.913
965 Thomsen, M.S., Routhe, L.J., Moos, T., 2017. The vascular basement membrane in the healthy and
966 pathological brain. J. Cereb. Blood Flow Metab. 37, 3300–3317.
967 doi:10.1177/0271678X17722436
968 Uchida, K., Reilly, M.P., Asakura, T., 1998. Molecular stability and function of mouse hemoglobins.
969 Zool Sci 15, 703–706. doi:10.2108/zsj.15.703
970 van Veluw, S.J., Hou, S.S., Calvo-Rodriguez, M., Arbel-Ornath, M., Snyder, A.C., Frosch, M.P.,
971 Greenberg, S.M., Bacskai, B.J., 2020. Vasomotion as a driving force for paravascular clearance
972 in the awake mouse brain. Neuron 105, 549–561.e5. doi:10.1016/j.neuron.2019.10.033
973 Wierenga, C.E., Clark, L.R., Dev, S.I., Shin, D.D., Jurick, S.M., Rissman, R.A., Liu, T.T., Bondi, M.W.,
974 2013. Interaction of age and APOE genotype on cerebral blood flow at rest. J. Alzheimers Dis.
975 34, 921–935. doi:10.3233/JAD-121897
976 Yamazaki, Y., Zhao, N., Caulfield, T.R., Liu, C.-C., Bu, G., 2019. Apolipoprotein E and Alzheimer
977 disease: pathobiology and targeting strategies. Nat. Rev. Neurol. 15, 501–518.
978 doi:10.1038/s41582-019-0228-7
979 Zhu, X., Bergles, D.E., Nishiyama, A., 2008. NG2 cells generate both oligodendrocytes and gray matter
980 astrocytes. Development 135, 145–157. doi:10.1242/dev.004895
981 Zlokovic, B.V., 2011. Neurovascular pathways to neurodegeneration in Alzheimer's disease and other
982 disorders. Nat. Rev. Neurosci. 12, 723–738. doi:10.1038/nrn3114
983 Zott, B., Simon, M.M., Hong, W., Unger, F., Chen-Engerer, H.-J., Frosch, M.P., Sakmann, B., Walsh,
984 D.M., Konnerth, A., 2019. A vicious cycle of β amyloid-dependent neuronal hyperactivation.
985 Science 365, 559–565. doi:10.1126/science.aay0198
986
987

988
989
990 Supplementary Information
991

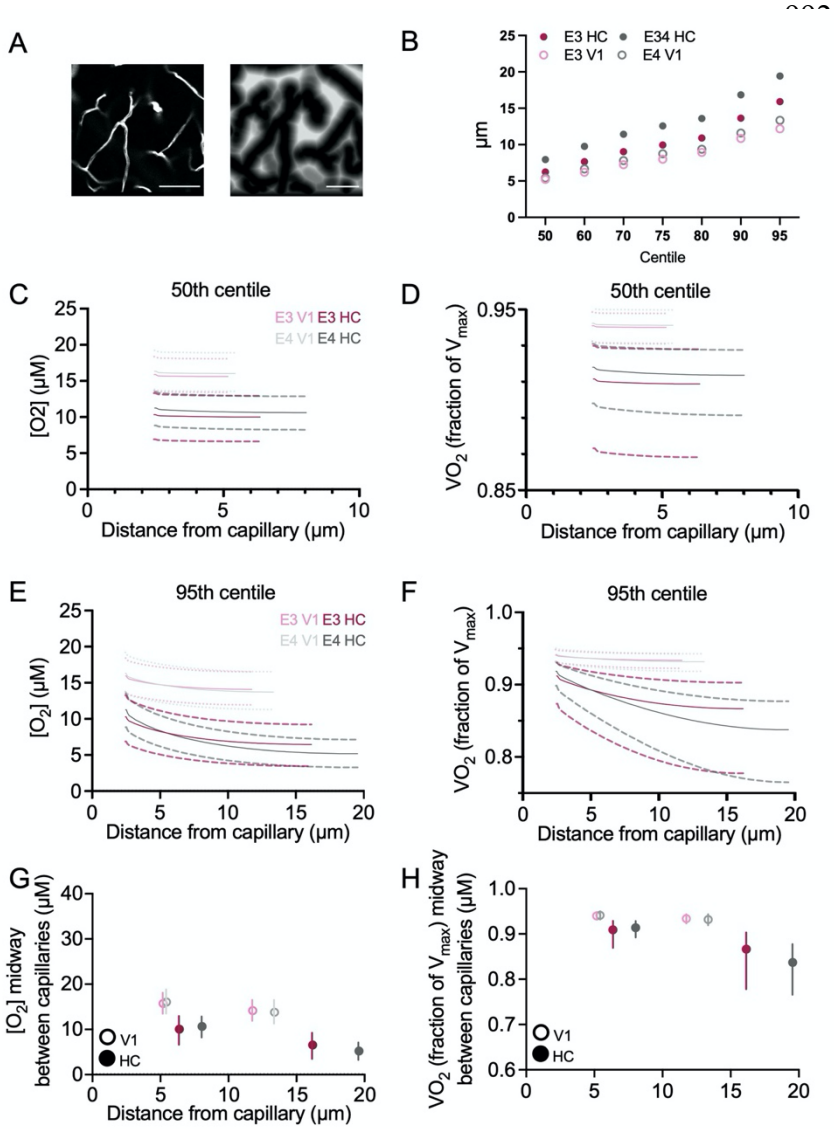

Figure 1: Supplementary Figure 1. Modelling O2 diffusion in brain tissue. ***(A)*** Distance maps of ***c***onfocal z-stacks of FITC-labelled vasculature from APOE3 or 4 visual cortex and hippocampus were used to calculate the distance of each parenchymal voxel from a vessel in each condition. Scale bar: 40µm. **(B)** The median distance of a parenchymal voxel and increasing centiles of the distribution were used in the diffusion model. Oxygen gradients across the **(C)** median and E) 95% centile distances were calculated using a simple model of oxygen diffusion and consumption, as described previously (Shaw et al., 2021a). Oxygen concentrations at the vessel were calculated from the median (solid lines) and upper and lower 95 % confidence intervals (dashed lines) for SO_2 measurements in APOE3 and APOE4 visual cortex and hippocampus, as described (Shaw et al., 2021a). **(D)** & **(F)** The rate of oxygen consumption in the tissue given these oxygen gradients was then calculated (VO_2, expressed as a fraction of the rate if oxygen levels were not limiting for ATP production), using the known oxygen-dependence of oxygen consumption by cytochrome c oxidase, as previously. Finally, the oxygen concentration **(G)** and VO_2 **(H)** for voxels at the median distance and 95% centile from a vessel are summarised. Error bars indicate models run with the 95% confidence intervals for SO_2 measurements in the different conditions. Despite the lower vascular density in APOE4 mice, when taking into account the measured blood oxygen levels, oxygen and VO_2 values are not predicted to be different in APOE3 and APOE4 mice in either the visual cortex or the hippocampus, based on the large overlap between genotypes of the 95% confidence intervals (Cumming and Finch, 2005), though as we found previously, both tissue oxygen levels and VO_2 values drop significantly lower in the hippocampus than the visual cortex. Open circles represent values from the visual cortex, whilst filled circles represent values from the hippocampus. Light pink and light grey lines represent values from the visual cortex and hippocampus of E3 mice respectively. Dark pink and dark grey lines represent values from the visual cortex and hippocampus of E4 mice respectively.
1027
1028
1029
1030
1031
1032
1033
1034
1035

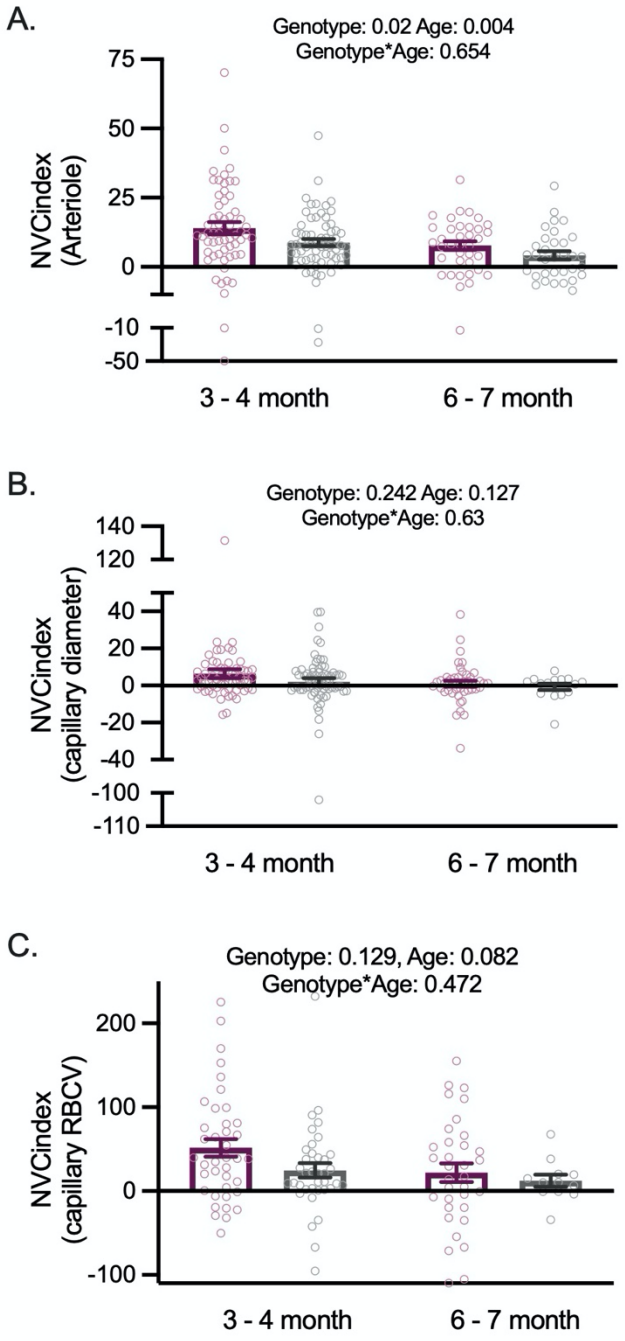

Figure 3: Supplementary Figure 1. Vascular response to visual stimulation normalised to average neuronal response to produce a neurovascular coupling index (NVCindexndex). Raised NVCindexndex in APOE3 animals was observed in pial arteriole **(A)** responses to visual stimulation**.** No difference was seen in capillary diameter **(B)** or RBCV NVCindex **(C).** Individual data points represent values from individual vessels. See appendix (i) for sample sizes and statistical tests.

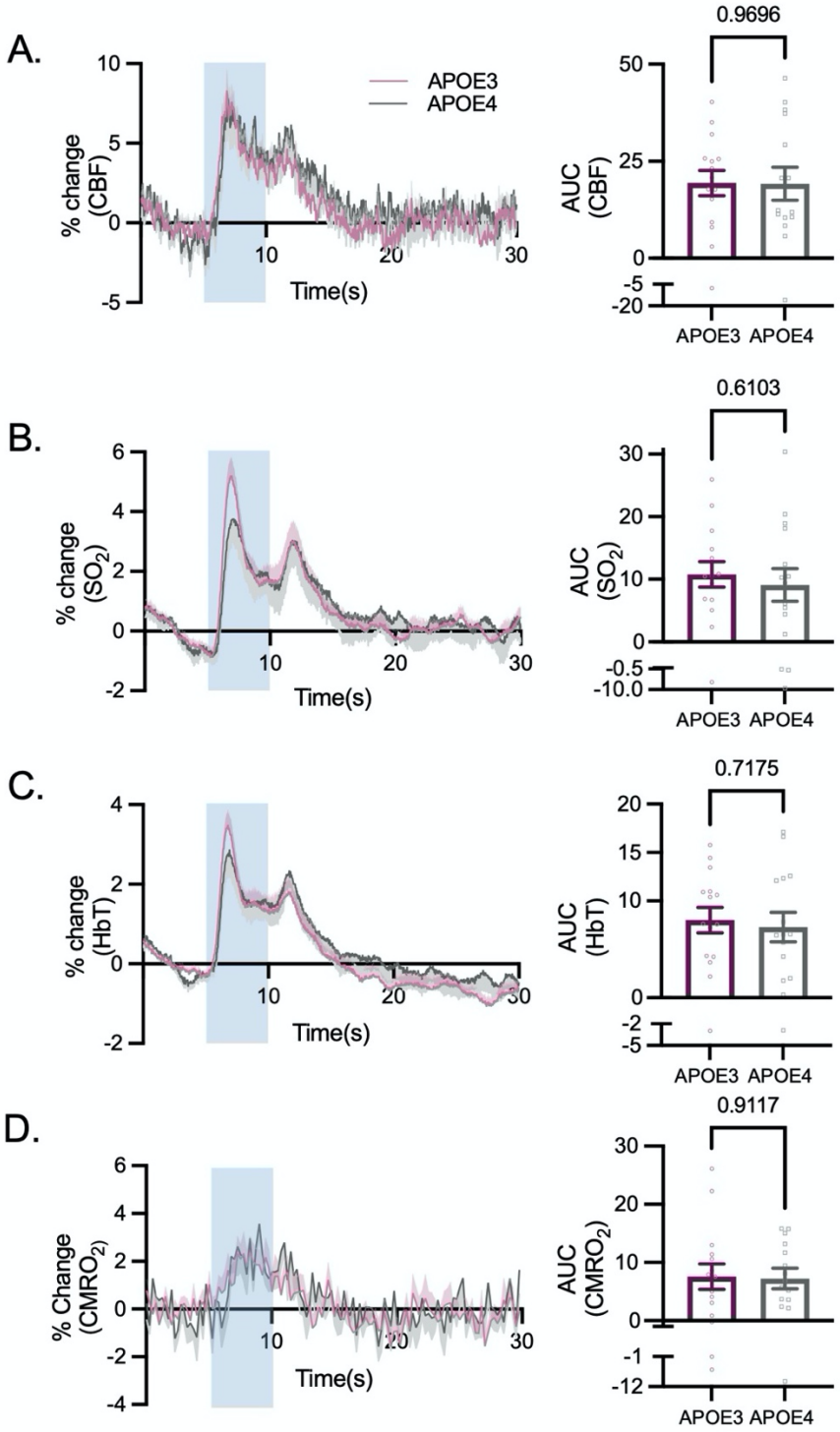

Figure 3: Supplementary figure 2. No effect of genotype was observed in net stimulus-dependent responses: Left panel shows average changes in net CBF **(A)**, sO_2 **(B)** total haemoglobin (HbT) **C)** and cerebral metabolice rate of oxygen consumption ($CMRO_2$); **D)** during 5s visual stimulation (blue shaded region). Right panel shows AUC for each during visual stimulation. Individual data points represent animal averages. See appendix (i) for sample sizes and statistical tests

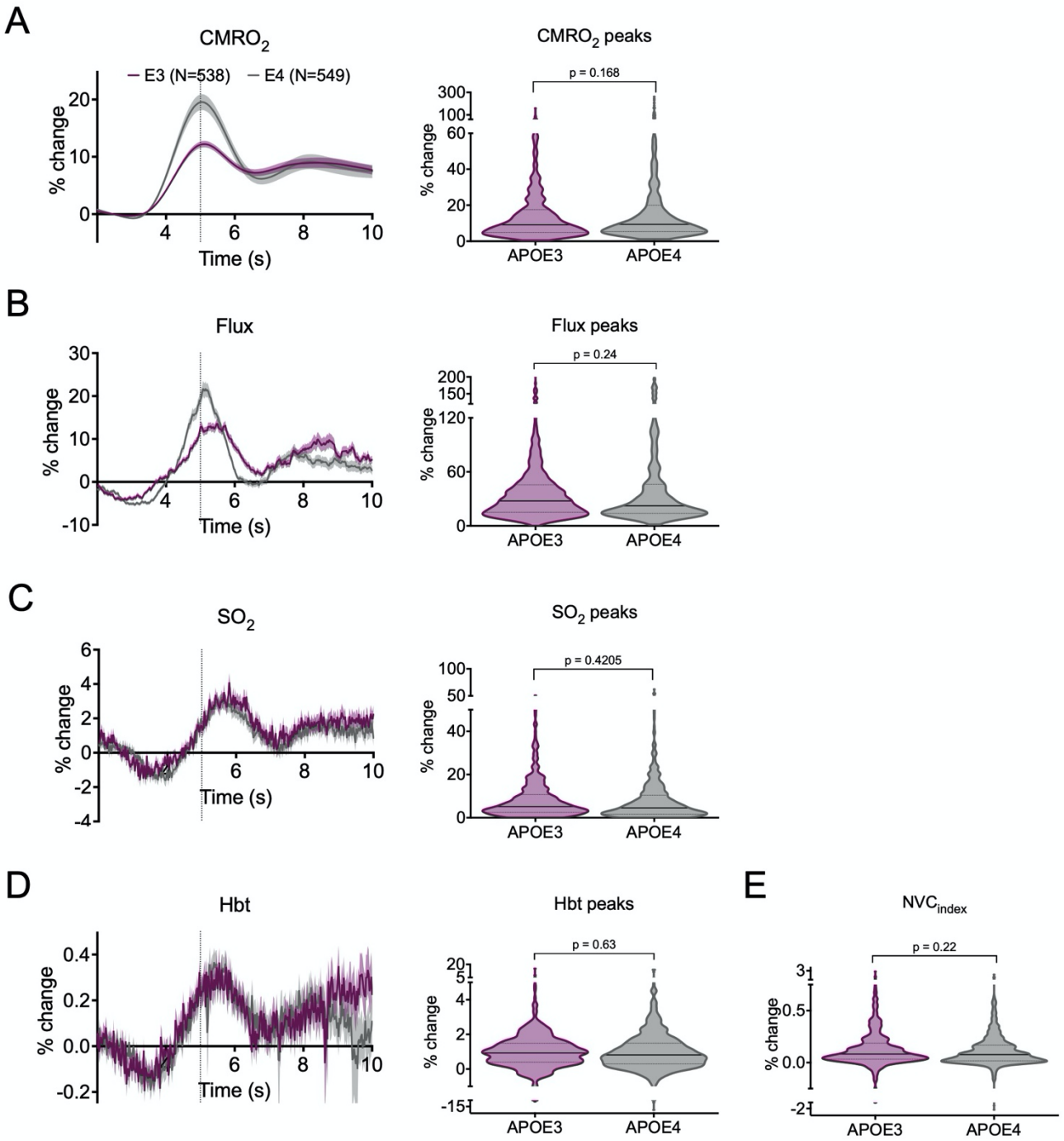

Figure 4: Supplementary Figure 1***: CMRO2-dependent haemodynamic responses in CA1***. **(A)** Detected peaks in CA1 Oxy-CBF probe recordings of net $CMRO_2$ were not larger in APOE4 than APOE3 mice, Corresponding CMRO2-dependent haemodynamic traces were then visualised for **(B)** flux, **(C)** oxygen saturation (SO_2) and **(D)** total haemoglobin (HbT). There were no significant genotype differences in CMRO2-dependent flux, SO_2 or HbT, **(E)** The NVCindexndex was calculated by dividing HbT/$CMRO_2$, and showed no effect of genotype. Violin plots are composed of data points from individual haemodynamic events. See appendix (i) for sample sizes and statistical tests.

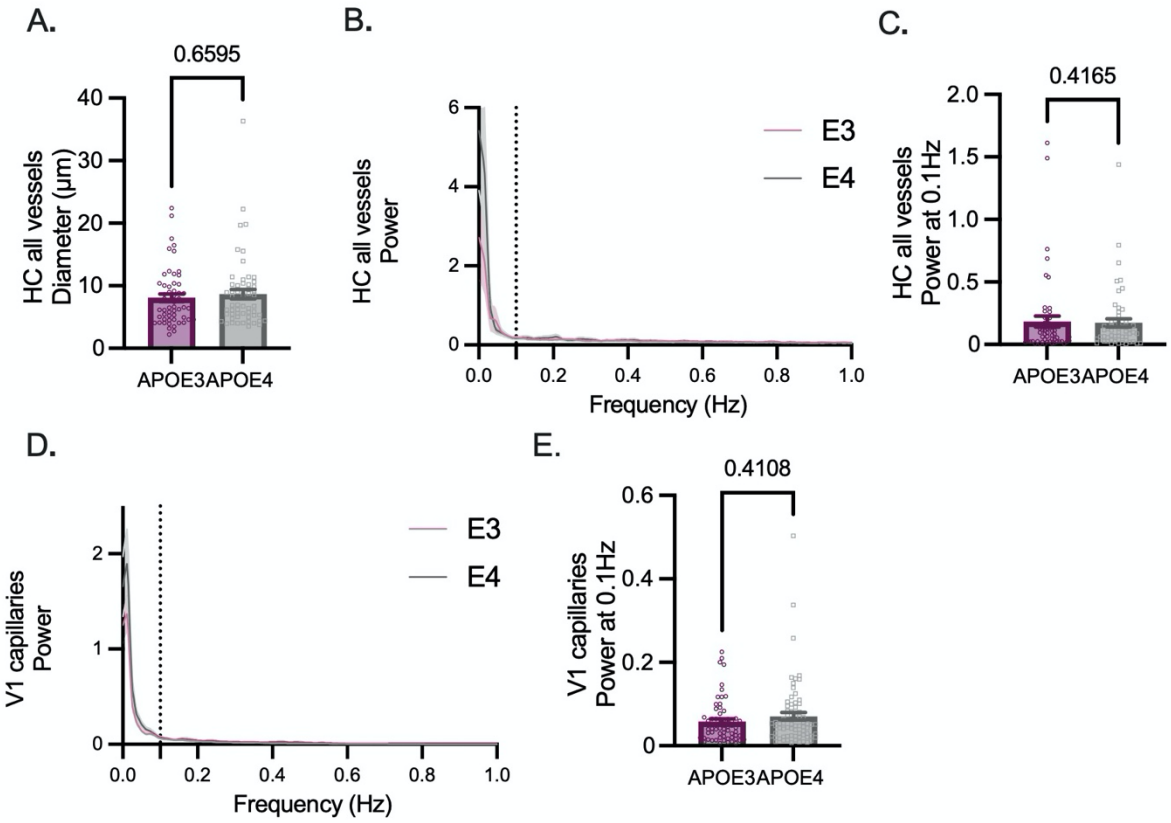

Figure 5: Supplementary Figure 1**: In APOE3 and APOE4 mice, power at the vasomotion frequency is the same in the vessels of the hippocampus and in the capillaries in V1**. The diameter of **(A)** all the vessels recorded in CA1 were not significantly different between genotypes. **(B)** Average power spectra of CA1 diameter traces from APOE3 (pink) and APOE4 (grey) mice for all recorded vessels. Dashed line at 0.1Hz. **(C)** Power at 0.1Hz did not differ between genotypes. **(D)** Average power spectra of V1 capillary diameter traces from APOE3 (pink) and APOE4 (grey) mice. **(E)** Power at 0.1Hz did not differ by genotype. See appendix (i) for sample sizes and statistical tests.

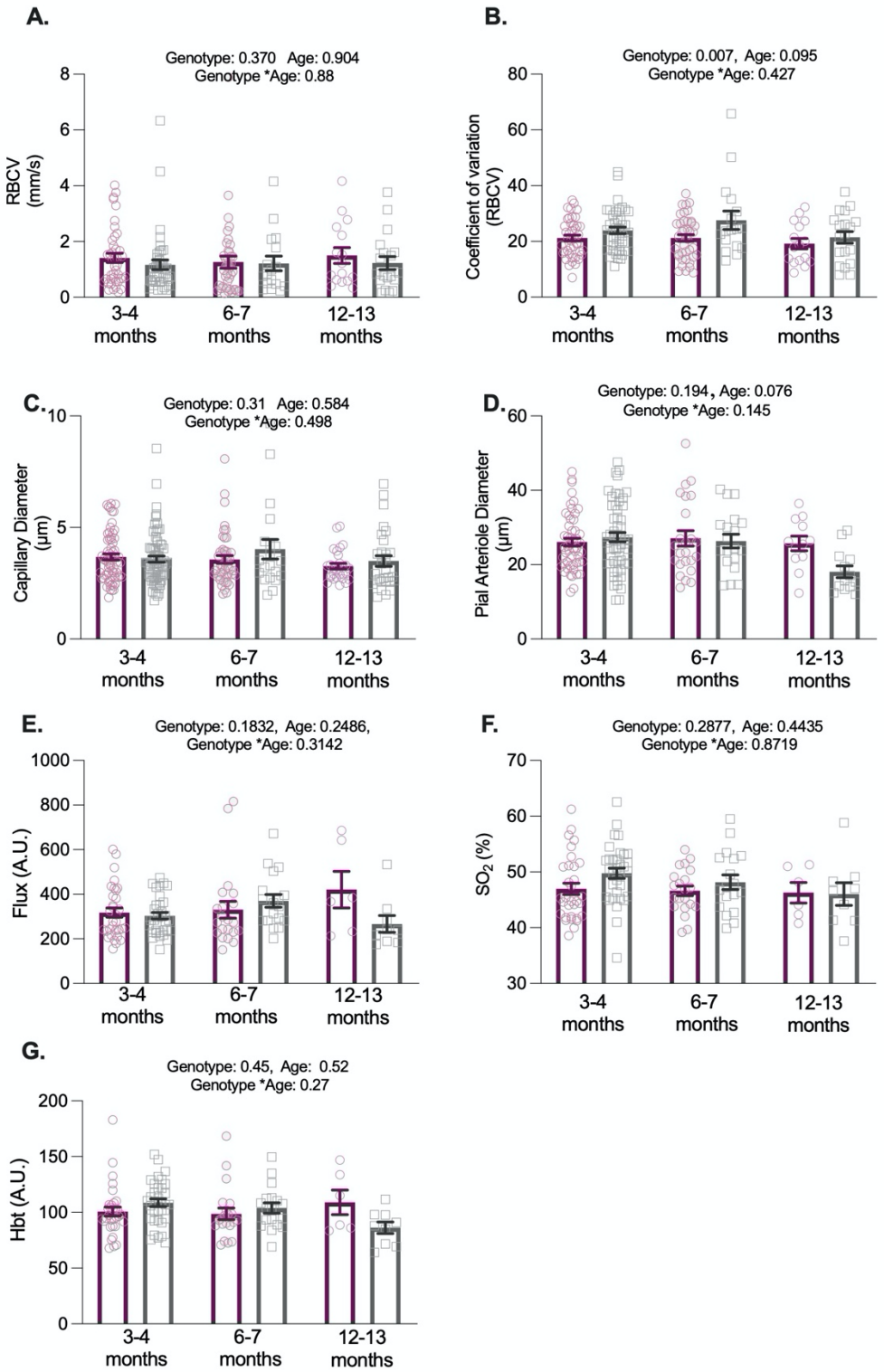

Figure 6: Supplementary Figure 1: ***Under baseline conditions functional measurements are largely preserved in APOE4 mice within brain regions. This effect is preserved in older animals.*** There was no effect of genotype or age on **(A)** RBCV, **(C)** capillary diameter, **(D)** arteriole diameter, **(E)** flux, **(F)** SO_2 or **(G)** HbT. However a significant effect of genotype was observed in RBCV CV measurements (B). Individual data points on bar graphs represent single vessels (A-D); or recording sessions (E-G). See appendix (i) for sample sizes and statistical tests.